A Design Method of Nonlinear Real-Time Optimal Controllers to Save Energy for Hybrid Electric Vehicle and Plug-In Hybrid Electric Vehicle Powertrains

余, 開江

https://doi.org/10.15017/1398397

出版情報：九州大学, 2013, 博士（学術）, 課程博士
バージョン：

A design method of nonlinear real-time optimal controllers to save energy for Hybrid Electric Vehicle and Plug-in Hybrid Electric Vehicle powertrains

by

Kaijiang Yu

A dissertation submitted in partial fulfillment
of the requirements for the degree of
Doctor of Philosophy
(Electrical and Electronic Engineering)
in Kyushu University
2013

Doctoral Committee:

Professor Taketoshi Kawabe, Chair

Professor Junichi Murata

Professor Masahito Shoyama

ABSTRACT

In recent years, more efficient and cleaner energy utilization technology has become a research hotspot due to the rising prices of fossil fuels and environmental problems. These lead to the development of hybrid electric vehicles (HEVs) and plug-in hybrid electric vehicles (PHEVs). HEVs combine the traditional internal combustion engine, the battery, and the motor/generator as their power plant. Compared with HEVs, PHEVs have an enlarged battery pack and can charge the battery using electricity from an electric grid with a plug. HEVs and PHEVs (referred as hybrid vehicles later) seem to be the main transitional products from internal combustion engine vehicles to battery electric vehicles (BEVs) in the near future. Hybrid vehicles can regenerate dissipation kinematic energy during deceleration and use the redundancy of hybrid vehicle power sources of the engine and the battery to regulate the engine operation to avoid low efficiency engine operating points. If the control method is properly designed, hybrid vehicles can get much more fuel economy improvements than those using conventional internal combustion engine vehicles (ICEVs). However, the engine optimal operating point depends on the property of the engine, the surrounding traffic conditions, the road slopes till the destination, and so on which change every moment. Also, if the battery is operated beyond the battery state of charge limits, this will lead the battery degradation and affect the battery longevity. In the conventional approach, feedback control

methods are presented with a formulation of the optimal control problem for known driving patterns till the destination. In this dissertation, the proposed method can optimize both the engine operating point and the driving profile with 30%-50% of fuel economy improvements by predicting future driving cycles, slopes, and traffic information. The topic is addressed in three phases according to the access level of knowledge of future loads.

First, fuel economy improvements in the HEV are confirmed by predicting daily commuting driving cycle information using the proposed nonlinear real-time optimal control method. The apparent relationship between the battery power and the future road load is addressed in the cost function of the fuel economy optimal control problem with a simplified HEV energy management system model. The fuel economy improvements using the proposed approach were confirmed quantitatively compared with those using the rule-based approach. The entire vehicle operating modes: idle stop, engine charge, engine start, electric vehicle, motor assist and electric continuously variable transmission, and regenerative braking, can be realized using the proposed real-time optimal control approach for HEVs.

Second, fuel economy optimization of HEVs is proposed by predicting future road slopes and traffic information. Considering the HEV physical constraints like the speed and torque limits of the engine and motor/generators, and the battery state of charge beforehand makes the optimization and the fuel improvements trustworthy. The real-time optimal control can consider constraints in advance. The performance index can be systematically designed. This systematic design process can be applicable to other fuel optimization problems. Using the HEV property, the desired battery state of charge is designed according to the road slopes for better recuperation of free regenerative braking energy. The fuel economy is improved due to this desired battery state of charge adaption. The proposed method gives the freedom of vehicle spacing between the preceding vehicle and the host vehicle. The vehicle spacing is

kept above the minimum value, and this gives the freedom of control for vehicle speed variety to get battery fuel economy. This freedom can improve the fuel economy. The superiority of the proposed nonlinear real-time optimal control approach was confirmed compared with the rule-based approach.

Third, the proposed method is extended when the driving distance is unknown. The fuel economy improvements for the PHEV are confirmed with driving distance uncertainty in reality using the proposed nonlinear real-time optimal control method. The proposed controller can be constructed without the trip distance information which is required in the conventional control method.

In total, this dissertation proposed a nonlinear real-time optimal control algorithm for energy management in HEVs and PHEVs. The main contribution is a systematic real-time optimal control approach for energy management in HEVs and PHEVs by predicting future road loads. This systematic design process is useful for significant fuel economy improvements in the energy management control unit application with minimal hardware cost. The conclusion is that the nonlinear real-time optimal control approach is effective for the energy management problem of the HEV/PHEV system.

DEDICATION

To the people who care about me, and look after me.

To my family.

ACKNOWLEDGMENTS

I am deeply grateful to my advisor, Professor Taketoshi Kawabe for the guidance, support, patience, and encouragement during the past three years. I cannot imagine a better role model using his action to lead me to grow in both academic and personal life. I appreciate this incredible fortunate opportunity very much. I would also like to thank my other committee members, Professor Junichi Murata and Professor Masahito Shoyama, for their helpful advice and comments.

I am great indebted to Dr. Masakazu Mukai for his key feedback on this project, through group laboratory meetings.

I am indebted to the Technical Committee on Automotive Control and Model Research (JSAE and SICE Joint) for their support in implementing the benchmark problem simulator. Especially I would like to thank Chief Engineer Yuji Yasui for his suggestions and ideas.

It is a great pleasure working in the System Design Laboratory as a doctoral student. I wish to thank Dr. Md. Abdus Samad Kamal, Dr. Anan Kaku, Peng Zhang, Wenjing Cao, Daisuke Yamaguchi, and other members, for their constructive critical suggestions, discussions, and moral support.

Finally, I want to thank the love and support of my family, my father Deming Yu, my mother Shirong Liu, my grandfather Xuezhi Liu, my grandmother Defang Yang, my younger

brother Kaihai Yu. I would also like to thank my fiancee, Qing Liang, for her encouragement, love, and support during these four years.

LIST OF PUBLICATIONS

K. Yu, M. Mukai, and T. Kawabe, "Model predictive control of a power-split hybrid electric vehicle system," *Artificial Life and Robotics*, vol. 17, no. 2, pp. 221–226, Dec. 2012.

K. Yu, M. Mukai, and T. Kawabe, "A battery management system using nonlinear model predictive control for a hybrid electric vehicle," Accepted in *the 7th IFAC Symposium on Advances in Automotive Control.*

K. Yu, M. Mukai, and T. Kawabe, "Model predictive control of a power-split electric vehicle system with slope information," Accepted in *the SICE Annual Conference 2013.*

TABLE OF CONTENTS

ABSTRACT ii

DEDICATION iv

ACKNOWLEDGMENTS v

LIST OF PUBLICATIONS vii

LIST OF FIGURES xi

LIST OF TABLES xv

LIST OF APPENDICES xvi

Chapter I. Introduction 1

1.1 Research Background and Motivation 2

1.2 Literature review 9

1.3 Key issues and main features of the approach 12

1.4 Contributions and research objective 14

1.5 Dissertation Organization 16

Chapter II. Fuel economy optimization for known daily commuting driving patterns **17**

2.1 Features of the approach for known daily commuting driving patterns 17

2.2 Modeling and control for the 1 degree of freedom model 18

2.3 Computer simulation results of the nonlinear real-time optimal control algorithm with daily commuting driving patterns for HEVs 25

2.4 Discussion for the simulation with known daily commuting driving pattern . 32

Chapter III. Driving cycle and engine operating point optimization for unknown driving patterns **34**

3.1 Features of the approach for unknown driving patterns 35

3.2 Modeling and control for the 3 degrees of freedom model 36

3.3 Simulation results for the unknown driving pattern with slope information . 46

3.3.1 Case 1 47

3.3.2 Case 2 49

3.4 Simulation results for the unknown driving pattern with slope and traffic information 54

3.4.1 Comparison controllers 54

3.4.2 Test road slope profiles and calculation of the road slopes and the desired battery state of charge 57

3.4.3 Simulation conditions 58

3.4.4 Simulation results 59

3.5 Discussion for the simulation for unknown driving patterns 69

Chapter IV. Optimal energy management of plug-in hybrid electric vehicles with uncertain driving distance **70**

4.1 Features of the approach with uncertain driving distance 70

4.2 modeling and control for the 1 degree of freedom model 71

4.3 Simulation results with uncertain driving distance 75

4.3.1 Comparison controllers 75

4.3.2 Simulation conditions 76

4.3.3 Simulation results 78

4.4 Discussion 82

Chapter V. Conclusions **87**

6.1 Conclusions 87

6.2 Future work 88

Appendices **90**

Bibliography **98**

LIST OF FIGURES

1.1.1 U.S. crude oil first purchase price (U.S. Energy Information Administration). 3

1.1.2 Monthly mean atmospheric carbon dioxide at Mauna Loa Observatory, Hawaii (National Oceanic & Atmospheric Administration). 3

1.1.3 Progression of European emission standards (European Commission). . . . 4

1.1.4 Prediction of vehicle transition in the near future, ICEV represents internal combustion engine vehicle, BEV represents battery electric vehicle (Graphic: [1]. 5

1.1.5 Graphic depiction of PHEV communication system (Graphic: Business Wire). 6

1.1.6 Hybrid vehicle configurations (Graphic: [9]) 7

1.1.7 PHEV control strategies. 8

1.3.1 The concept of the nonlinear real-time optimal control for HEV powertrains with slope and traffic information. 14

2.2.1 Model of the hybrid electric vehicle. Diagram adapted from [9] 19

2.2.2 The proposed HEV energy management approach 23

2.3.1 The engine OOL of the HEV system 27

2.3.2 Simulation results of the benchmark problem rule-based approach 28

2.3.3 Simulation results of the nonlinear real-time optimal control approach . . . 29

2.3.4 Engine operating point distribution using the benchmark problem rule-based approach 30
2.3.5 Engine operating point distribution using the nonlinear real-time optimal control approach 30
2.3.6 Detailed simulation results of the benchmark problem rule-based approach . 31
2.3.7 Detailed simulation results of the nonlinear real-time optimal control approach 31
3.2.1 Structure of the nonlinear real-time optimal control system. 45
3.3.1 Driving profile of the real-time optimal control algorithm and the ASCD algorithm in Case 1. 49
3.3.2 Power-split profile of the vehicle using the real-time optimal control algorithm in Case 1. 50
3.3.3 Power-split profile of the vehicle using the ADVISOR rule-based algorithm in Case 1. 51
3.3.4 Engine operating point distribution using the real-time optimal control algorithm and the ADVISOR rule-based algorithm in Case 1. 52
3.3.5 Driving profile of the real-time optimal control algorithm and the ASCD algorithm in Case 2. 53
3.3.6 Power-split profile of the vehicle using the real-time optimal control algorithm in Case 2. 54
3.3.7 Power-split profile of the vehicle using the ADVISOR rule-based algorithm in Case 2. 55
3.3.8 Engine operating point distribution using the real-time optimal control algorithm and the ADVISOR rule-based algorithm in Case 2. 56
3.4.1 Flowchart of the nonlinear real-time optimal control algorithm. 61

3.4.2 Driving profile of the vehicle tracking nonlinear real-time optimal control algorithm and the ACC algorithm. PV represents the preceding vehicle, HV represents the host vehicle. 63
3.4.3 Power-split profile of the vehicle using the solitude real-time optimal control algorithm. 64
3.4.4 Power-split profile of the vehicle using the fixed desired battery SOC vehicle tracking real-time optimal control algorithm. 64
3.4.5 Power-split profile of the vehicle using the vehicle tracking nonlinear real-time optimal control algorithm. 65
3.4.6 Power-split profile of the vehicle using the vehicle tracking ADVISOR rule-based algorithm. 65
3.4.7 Engine operating point distribution using the solitude real-time optimal control algorithm and the solitude ADVISOR rule-based algorithm. The crosses and the circles denote the engine operating points of the solitude real-time optimal control algorithm and the solitude ADVISOR algorithm, respectively. 66
3.4.8 Engine operating point distribution using the vehicle tracking nonlinear real-time optimal control algorithm and the car tracking ADVISOR rule-based algorithm. The crosses and the circles denote the engine operating points of the vehicle tracking nonlinear real-time optimal control algorithm and the vehicle tracking ADVISOR algorithm, respectively. 66
3.4.9 Engine operating point distribution using the fixed desired battery SOC vehicle tracking real-time optimal control algorithm. 67

4.3.1 State-of-charge response for the blended and CDCS control strategies on two FTP-72 cycles simulated back-to-back. The blended control strategy is the same as the charge depletion control strategy is this work. Figure referred to [8] 79
4.3.2 Simulation results of the nonlinear real-time optimal control CD approach . 80
4.3.3 Simulation results of the nonlinear real-time optimal control CDCS approach 81
4.4.1 Engine operating points for the blended strategy on a brake specific fuel consumption map, for two FTP-72 cycles simulated back-to-back. The blended control strategy is the same as the charge depletion control strategy is this work. Figure referred to [8] 84
4.4.2 Engine operating points for the CDCS strategy on a brake specific fuel consumption map, for two FTP-72 cycles simulated back-to-back. Figure referred to [8] 84
4.4.3 Engine operating point distribution using the nonlinear real-time optimal control CD approach 85
4.4.4 Engine operating point distribution using the nonlinear real-time optimal control CDCS approach 85
4.4.5 Detailed simulation results of the nonlinear real-time optimal control CD approach 86
4.4.6 Detailed simulation results of the nonlinear real-time optimal control CDCS approach 86
6.0.1 The engine efficiency map to the best engine operating points 92
6.0.2 The engine efficiency curve to the best engine operating points 93
6.0.3 The engine fuel consumption rate to the best engine operating points 93

LIST OF TABLES

2.3.1 Fuel economy comparison results for daily commuting driving patterns, where T is the prediction horizon, ACT represents average computation time per sampling interval, and MCT represents max computation time per sampling interval. 32

3.3.1 Fuel economy comparison results for the unknown driving pattern with slope information 53

3.4.1 Fuel economy comparison results for the unknown driving pattern with slope and traffic information 68

4.3.1 Fuel economy comparison results 82

LIST OF APPENDICES

APPENDIX A: ENGINE FUEL CONSUMPTION MODEL 91

APPENDIX B: SOLUTION OF THE REAL-TIME OPTIMAL CONTROL PROBLEM 94

CHAPTER I

Introduction

This dissertation addresses nonlinear real-time optimal control algorithms that utilize preview information of driving cycles, road slopes, and surrounding vehicles aiming at fuel economy optimization for hybrid electric vehicles (HEVs) and plug-in hybrid electric vehicles (PHEVs). This research subject is motivated by the need to develop more efficient and cleaner hybrid vehicles due to the energy deficit and stricter and stricter emission regulations. The method is the usage of the redundancy of HEV/PHEV power sources to optimize both the engine operating point and the driving profile. However, the hybrid vehicle system is nonlinear because of nonlinearity of battery, engine, motor/generator dynamics, and the performance index. Also, the future road loads due to road slopes, surrounding traffic situations, and so on, change every moment. Therefore, Real-time optimal control is needed for on-line computation due to the unknown of future road loads and the constraints of the power-train components. On-line control of hybrid vehicles was not emphasized in the past because of difficulty of prediction of future loads. In the last few decades, vehicle navigation technology using GPS, digital map databases, and laser sensors have been developed quickly. This promotes information usage in the energy management of HEVs and PHEVs. This dissertation focuses on software design using preview information like road slopes, trip

information, and traffic information to optimize fuel economy. The proposed real-time optimal control algorithms have the potential for real-time implementation of hybrid vehicle control with only software changes. The proposed algorithms computed on-line addresses the energy management problem with predicted driving behavior instead of predefined driving cycles. This problem has not been generally explored in the literature.

The remainder of this introduction is structured as follows. First, the research background and motivation are presented. Second, the existing literature concerning this work is reviewed. Third, key issues and main features of the approach are presented. Fourth, the contributions and objective of this work are summarized. Finally, the outline of this dissertation is provided.

1.1 Research Background and Motivation

In recent years, more efficient and cleaner energy utilization technology has become a research hotspot due to the rising prices of fossil fuels and environmental problems. The price of crude oil increases very much in the past (Fig. 1.1.1). The transportation sector accounts for a big part of all the crude oil use. The carbon dioxide emission increases affect the global environment a lot. The monthly mean atmospheric carbon dioxide at Mauna Loa Observatory, Hawaii, is shown in Fig. 1.1.2. To solve the above problems, it is required to develop more efficient and cleaner vehicles.

Concurrent with fuel economy improvement requirements is the more and more stringent emission standards. Fig. 1.1.3 shows the progression of European emission standards. The automotive industry faces challenges of improving vehicle fuel economy and reducing emissions.

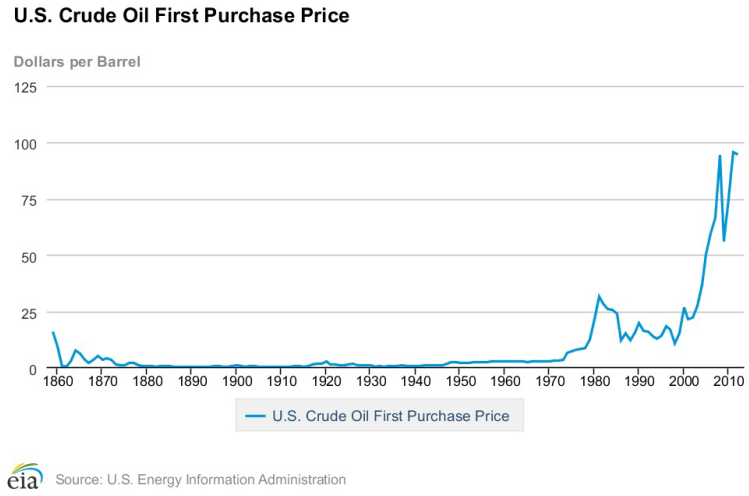

Figure 1.1.1: U.S. crude oil first purchase price (U.S. Energy Information Administration).

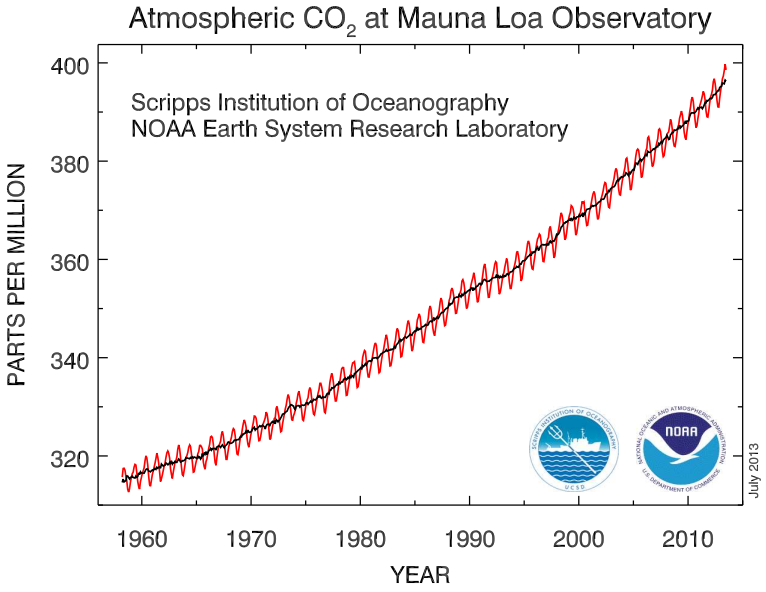

Figure 1.1.2: Monthly mean atmospheric carbon dioxide at Mauna Loa Observatory, Hawaii (National Oceanic & Atmospheric Administration).

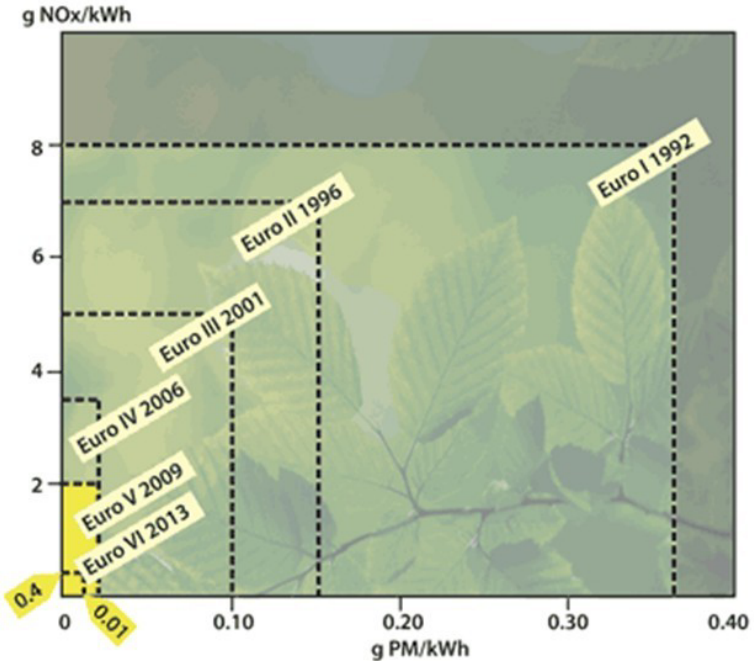

Figure 1.1.3: Progression of European emission standards (European Commission).

These lead to the development of more fuel efficient hybrid vehicles. Fig. 1.1.4 shows the prediction of vehicle transition in the near future [1]. Hybrid electric vehicles and plug-in hybrid electric vehicles seem to be the transitional products from internal combustion engine vehicles to battery electric vehicles (BEVs). HEVs are promising short-term solutions due to their independence from charging stations. Charging infrastructure has been developed quickly recently. Plug-in hybrid electric vehicles may be a long-term solution to the above problems in the future 40 years from today's viewpoint. PHEVs have been on sale for years. Hadley and Tsvetkova [2] estimate that by 2030 the market share of BEVs/PHEVs could reach 25%. Compared with traditional HEVs, BEVs/PHEVs have an enlarged battery pack and an intelligent converter [3]. Intelligent converter is a kind of converter to regulate the battery voltage to control the speed of the motor according to some intelligent control algo-

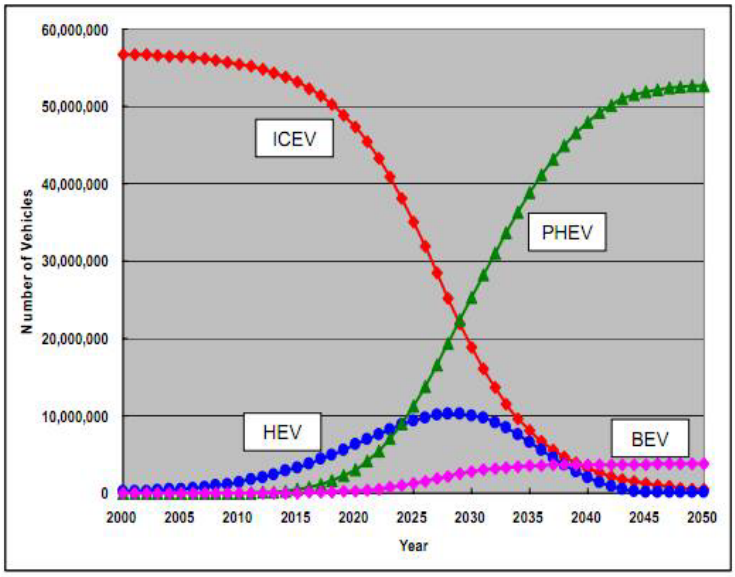

Figure 1.1.4: Prediction of vehicle transition in the near future, ICEV represents internal combustion engine vehicle, BEV represents battery electric vehicle (Graphic: [1].

rithms. Using a plug, BEVs/PHEVs can charge the battery using electricity from an electric power grid, also referred to as "grid-to-vehicle" (G2V) operation, or discharge it to an electric power grid during the parking hours, also referred to as "vehicle-to-grid" (V2G) ([4]– [5]) operation. With the introduction of a smart garage, which represents an interface between the transportation network and electric power system, the vehicle charging/discharging infrastructure and control system can be available widely making the proposed vehicle to building (Fig. 1.1.5) idea viable and economically attractive [6]. A PHEV uses a battery to add an extra degree of freedom for the power sources. It can downsize the internal combustion engine, optimize the engine operating point, use the battery electricity obtained by plugging into the electric grid, and regenerate dissipation kinematic energy during deceleration, which help to improve fuel economy and reduce emissions [7], [8].

There are three kinds of hybrid vehicles. They are parallel hybrid vehicles, series hybrid

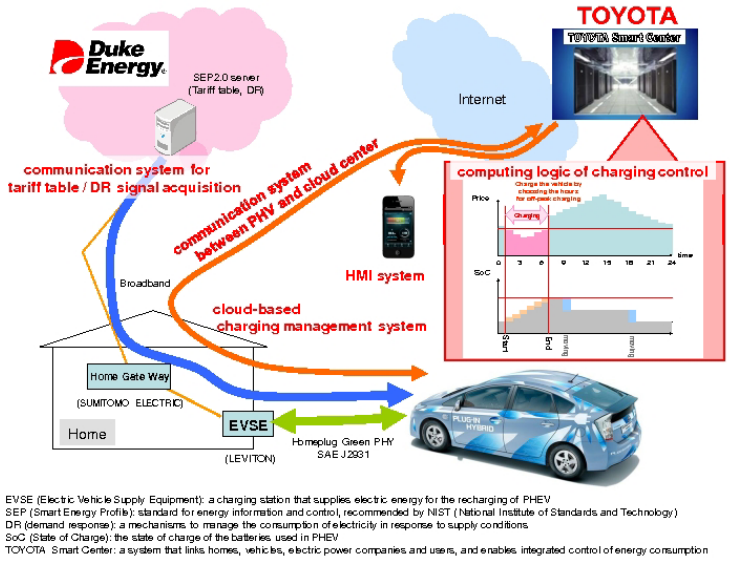

Figure 1.1.5: Graphic depiction of PHEV communication system (Graphic: Business Wire).

vehicles and power-split hybrid vehicles (Fig. 1.1.6). Parallel hybrid vehicles have mechanical and electric paths to drive the vehicle. Series hybrid vehicles use the engine to generate electricity to drive the vehicle. Power-split hybrid vehicles combine parallel hybrid vehicles and series hybrid vehicles with a power-split device. The main drawback of the parallel configuration is that it has only a single electrical machine. The battery assisting vehicle driving or the engine charging battery must be selected. As for series hybrid vehicles, since the engine operation is independent of the vehicle speed and road loads, it can be operated near its optimal condition. A disadvantage of such a configuration is that the electric machines will reduce the overall power-train efficiency. The power-split hybrid vehicle has functionality of both series and parallel hybrid vehicles, and it has more modes to get better fuel economy. It can split the engine power into a mechanical path and an electrical path. Assuming the vehicle speed is constant, using the generator, the engine speed can be adjusted according to the engine optimal operating line. Using the generator the power split device can move

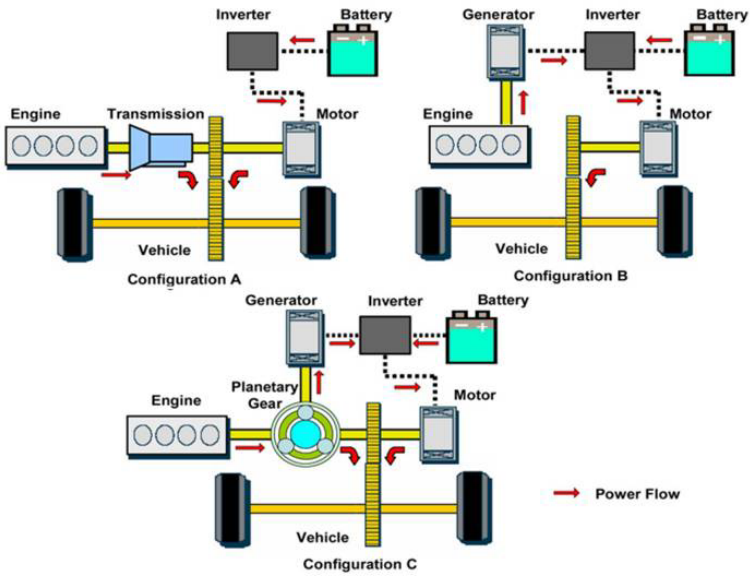

Figure 1.1.6: Hybrid vehicle configurations (Graphic: [9])

the engine operating point to the engine optimal operating line.

The key technology of PHEVs is its energy management. There are two kinds of control strategies for PHEVs: charge depletion and all-electric charge depletion followed by charge sustenance (see Fig. 1.1.7). The charge sustenance strategy for PHEVs is similar to that for HEVs. The authors of [10] proposed a charge depletion strategy. This strategy can get better fuel economy compared with the all-electric charge depletion followed by charge sustenance control strategy. However this fuel economy improvement is possible if the trip distance has been predetermined for the strategy through either user input or algorithmic prediction. In order not to use the trip distance information, this study presents a control algorithm to operate the engine near the engine best efficiency line. When the trip distance and the driving cycle are known, the charge depletion strategy may be the best control strategy. When the trip distance and the driving cycle are not known, the all-electric charge

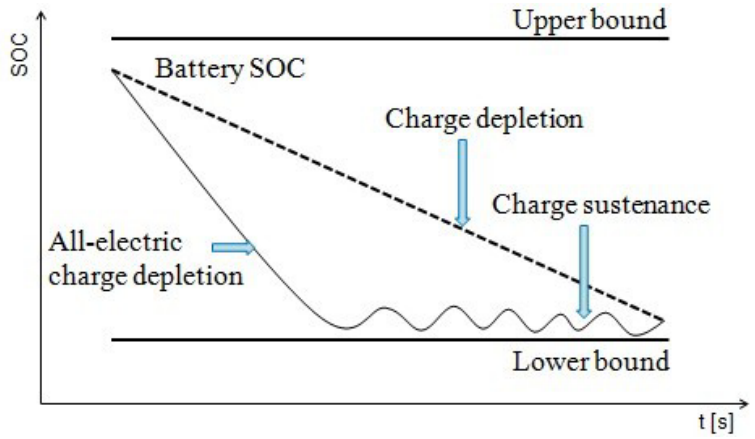

Figure 1.1.7: PHEV control strategies.

depletion followed by charge sustenance strategy may be the best control strategy. PHEVs are extension products of hybrid electric vehicles. Although a PHEV is similar to an HEV, it needs to have a high capacity battery and a new control strategy that manage the connection with the smart home and the smart grid. To make good use of the smart grid and the smart home, the PHEV battery state of charge needs to be scheduled properly to deplete the battery charge to the expected values, when the PHEV reaches the home or the charging station. Since PHEVs have two energy sources i.e. gasoline energy and battery energy that is larger than BEVs' to be planned. PHEVs have more flexibility to be controlled than BEVs. Therefore PHEVs can match for the smart grid use and the smart home use. Using the real-time optimal control algorithm, PHEVs can get better fuel economy with causality, and can deal with uncertainties like destination changes, road slopes, traffic conditions, and so on. An HEV maintains the battery's state of charge (SOC) in a narrow operating band during the whole trip. However, in a PHEV maximum energy efficiency is achieved if the batteries are depleted to their minimum allowable charge by the end of the trip [11].

1.2 Literature review

A lot of works have been published on the energy management problem of HEV systems. These approaches are typical in a family of optimal control techniques [12]– [24]. They can be subdivided into four categories: numerical optimization, analytical optimal control theories, instantaneous optimization, and heuristic control techniques [25]. The most representative of numerical optimization is dynamic programming (DP) [25]– [34]. However DP is based on fixed speed patterns which are impossible to get in reality. A kind of analytical optimal control techniques is Pontryagin's minimum principle [35]– [39]. It gives necessary conditions that the optimal solution must satisfy. It also needs to know the entire driving cycle in advance. The instantaneous optimization includes the equivalent consumption minimization strategy (ECMS) [40]– [43]. It is based on instantaneous optimization and is easy to implement in real-time. However it cannot guarantee the optimality over the whole driving cycle. Heuristic control techniques like rule-based control strategies [44] are robust, but they are impossible to guarantee the optimality. In [45], dynamic programming, quadratic programming, and model predictive control (MPC) [46]– [53] solutions of HEV energy management problems were presented. A model predictive control approach was used to investigate the energy management problem of a power-split HEV over standard driving cycles in [54]– [57]. A new charge/discharge control system for hybrid electric vehicles based on the use of car navigation information was proposed in [58].

The literature related to PHEV energy management problems provides a lot of approaches using the ideas to model and control the powertrain components for better fuel economy. A stochastic optimal control approach for power management in plug-in hybrid electric vehicles was proposed by [8]. A comparison of plug-in hybrid electric vehicle control strategies EV

and charge-depleting was presented by [10]. Energy-optimal control of plug-in hybrid electric vehicles for real-world driving cycles was proposed by [59]. The Gipps car following model was applied to the local road trip modeling of plug-in hybrid electric vehicle power management using historical traffic data on flat roads in [60]. The authors of [61] proposed a new approach to optimal power management of plug-in hybrid electric vehicles in the charge-depletion mode with driving cycle modeling based on the historic traffic information. Both dynamic programming and the equivalent consumption minimization strategy (see [62]– [71]) were utilized to optimize the battery state of charge profile with terrain, vehicle speed, and trip distance information for a PHEV power management problem in [11].

Although model predictive control is also in the numerical optimization class, its advantage is its predictive nature. The method can use road traffic information in the near future [58] and be applicable to the unfixed speed pattern [72]– [80]. Based on a simple and accurate model of the system, MPC can provide real-time control for the system. This work refers the model predictive control which has the ability for on-line computation as real-time optimal control. This dissertation examines energy management problems of both HEVs and PHEVs. The fuel economy optimization results of HEVs/PHEVs rely strongly on the future road load. The battery SOC can be scheduled optimally using the future road load. The main part of future road loads in cities is relevant to the car following situation. The main part of future road loads between cities depends on the road slope.

When the slope information in advance is predicted, the battery can be depleted slowly in the PHEV case, or be charged up in the HEV case, before the upslope. So the HEV/PHEV can make best use of the battery charged power to assist the vehicle driving. Then the battery SOC is reduced to be prepared for the upcoming downhill battery charging. At last the battery is charged up by the free regenerative braking energy. These make better use of

the high efficiency points of the engine and the regenerative braking energy. The preceding vehicle is assumed to be equipped with an ecological driver-assistance system developed by the authors of [73], and is controlled by a nonlinear model predictive controller proposed by the authors of [81], [82]. Since ordinary drivers have some intelligence, it is more reasonable to assume an eco-driving preceding vehicle (PV) than a conventional proportional-integral controlled preceding vehicle. For example, a driver will accelerate the vehicle before the up slope, and decelerate the vehicle before the down slope to make good use of the vehicle inertia kinetic energy. This intelligent driver behavior was realized by [81]. When this preceding vehicle eco-driving behavior is predicted, the following vehicle can schedule the speed and the vehicle spacing optimally using a nonlinear real-time optimal control approach. Especially for MPC, the future road load can be incorporate in the predictive model to better optimize the future speed profile and energy use. In other words, a decentralized nonlinear real-time optimal control system can be developed to model more real vehicle driving situations to get better fuel economy.

Recently, the vehicle GPS-based navigation technology, digital map databases, and laser sensors have been developed quickly. Prediction of future vehicle road loads like road slopes, and preceding vehicle position and speed is becoming realistic, which was impossible in three decades ago. Research on look-ahead control using the GPS road slope information for the fuel optimization of a conventional powertrain heavy truck was accomplished in [83]. A novel development of an ecological driving system for an internal combustion engine vehicle with a continuously variable transmission (CVT) on roads with up-down slopes using a digital map database was presented in [73]. Both dynamic programming and the equivalent consumption minimization strategy were utilized to optimize the battery state of charge profile with terrain information for an HEV power management problem in [40]. For adaptive cruise

control (ACC), the emphasis is on safely increasing driving comfort rather than increasing road capacity. Therefore normally a constant headway or other safe following policies is used to determine the following distance [84]. In [85], two different longitudinal control policies for automatically controlled vehicles were investigated. One was based on maintaining a constant spacing between the vehicles while the other was based upon maintaining a constant headway (or time) between successive vehicles. In the work [81], a nonlinear model predictive control algorithm using a simplified model for a power-split HEV was proposed to optimize the vehicle speed profile and the fuel economy. The engine is assumed always worked along its optimal operating line which was an industrial traditional energy management strategy for commercially available HEVs in [86]. Instead of the above general rule, searching whole areas of the engine fuel consumption map for better fuel economy is also investigated in this work.

Eco-driving involves such things as accelerating moderately (with shift ups between 2000 and 2500 revolutions for those with manual transmissions), anticipating traffic flow and signals, thereby avoiding sudden starts and stops; maintaining an even driving pace (using cruise control on the highway where appropriate), driving at or safely below the speed limit; and eliminating excessive idling defined by [87]. As for this work, the eco-driving is represented by the fuel reduction. The fuel economy is calculated using the fuel consumption during a certain time interval.

1.3 Key issues and main features of the approach

Three key issues of nonlinear real-time optimal controller design to save energy for HEV and PHEV powertrains are addressed in this dissertation.

The fist issue is the fuel economy optimization problem for the daily commuting driving cycle. Much of vehicle use is for commuters. The daily commuting driving cycle is usually known. Fuel economy optimization of this kind of vehicles can save much energy. Especially for hybrid vehicles which have the redundancy of power sources using the engine and the battery, the fuel economy can be much better by operating the engine optimally. Also, the battery can regenerate dissipation kinematic energy during deceleration for better fuel economy using the known driving pattern. However, there is a problem that if the battery works beyond the SOC bounds, this will cause the degradation of the battery and affect the longevity of the battery. The feature of the proposed approach is the consideration of the battery SOC constraint in advance and the adaptation of the battery power according to the vehicle power demand. The nonlinear real-time optimal control approach has the advantage for dealing with constraints in a predictive control structure. A new cost term is designed to make best use of the battery for better fuel economy.

The second issue is the fuel economy optimization problem for the unknown driving pattern. In reality, the driving pattern is always unknown. Even in the daily commuting driving cycle, there is some deviation between the prescribed vehicle speed and the real vehicle speed. The power fluctuations because of road slopes, surrounding traffic conditions, and other uncertain situations make the fuel economy optimization difficult. The feature of the proposed approach is that both the driving cycle profile and the engine operating point are optimized. Another new feature of the proposed is that the proposed control has the freedom of vehicle spacing between the preceding vehicle and the host vehicle. The vehicle spacing is kept above the minimum value, and this gives the freedom of control for vehicle speed variety to get battery fuel economy. Also, the proposed approach has the feature that using the HEV property, the desired battery state of charge is designed according to the road

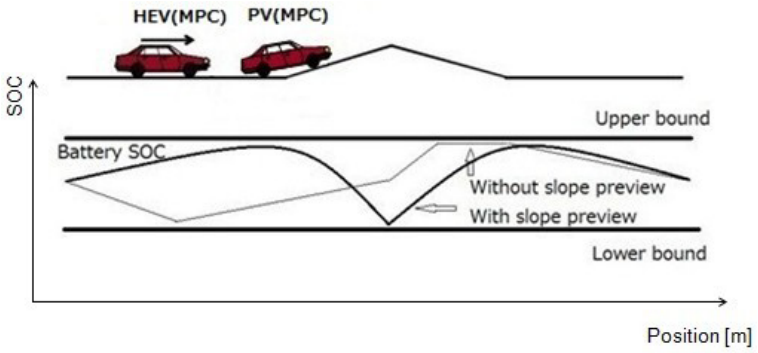

Figure 1.3.1: The concept of the nonlinear real-time optimal control for HEV powertrains with slope and traffic information.

slopes for better recuperation of free braking energy using digital maps (see Fig. 1.3.1).

The third issue is the fuel economy optimization problem for the uncertain driving distance for PHEVs. The driving distance affects the large battery energy usage. However, in reality, the driving distance is always uncertain. This makes the engine operating point optimization difficult. This work proposes a new control approach which makes usage of trip distance information unnecessary. The feature of the proposed approach is that the proposed controller can be constructed without the trip distance information which is required in the conventional control method. This is realized by optimizing the engine optimal operating point near the engine optimal operating line.

1.4 Contributions and research objective

This dissertation provides the solution to the problem based on JSAE-SICE Benchmark problem 2: fuel economy optimization of a commuter vehicle with a hybrid powertrain [88] and [89] provided by the Technical Committee on Automotive Control and Model Research

(JSAE and SICE Joint). Research on known and unknown vehicle speed patterns is investigated in this work. This paper extends HEV/PHEV energy management research by adding five novel contributions.

First, all of the vehicle operating modes: idle stop, engine charge, engine start, electric vehicle, motor assist and electric continuously variable transmission, and regenerative braking [88] and [89], can be realized using the proposed real-time optimal control approach compared with parts of vehicle operating modes using conventional algorithms [90] and [91]. Vehicles need to adapt to various road loads, therefore, a systematic and causal process of vehicle modeling and control which can be applied to the various vehicle operating modes is necessary.

Second, considering the HEV/PHEV physical constraints like the speed and torque limits of the engine and motor/generators, and the battery state of charge beforehand makes the optimization and the fuel improvements trustworthy. The proposed approach uses logarithm functions to deal with the state constraints and the state variant control input constraint which are required to be dealt in real-time. The nonlinear real-time optimal control approach can consider constraints in real-time.

Third, the modeling and control method can be systematically designed. By analyzing the configuration of the power-split hybrid electric vehicle system, a 3 degrees of freedom control oriented model is developed. The controller is constructed considering just the control objectives and the system constraints which is a nature and causal design process. This systematic design process can be applicable to other fuel optimization problems for HEVs and PHEVs.

Fourth, the proposed method gives the freedom of vehicle spacing between the preceding

vehicle and the host vehicle. The vehicle spacing is kept above the minimum value, and this give the freedom of control for vehicle speed variety to get battery fuel economy. This freedom can improve the fuel economy. This freedom can be obtained by the real-time optimal control.

Fifth, using the HEV property, the desired battery state of charge is designed according to the road slopes for better recuperation of free regenerative braking energy. It is not good for the HEV fuel economy if the HEV reaches the top of a hill with a fully charged battery. It is difficult to obtain the desired battery state of charge profile from the optimization view. The fuel economy is improved due to this desired battery state of charge adaption.

The objective of this work focuses on developing systematic utilization of nonlinear real-time optimization control methods for HEVs and PHEVs over known and predicted vehicle speed patterns including preview information such as trip information, road slopes, and traffic information.

1.5 Dissertation Organization

The organization of this dissertation is as follows. Chapter I presents the introduction. Chapter II presents the modeling, control, and simulation of hybrid electric vehicles for known daily commuting driving patterns. This model is control oriented for future road load predictions. Chapter III introduces the modeling, control, and simulation of hybrid electric vehicles for unknown driving patterns with both driving cycle optimization and engine operating point optimization. Chapter IV provides the modeling, control, and simulation of plug-in hybrid electric vehicles with uncertain driving distance. Chapter V summarizes the conclusions and possible future research directions.

CHAPTER II

Fuel economy optimization for known daily commuting driving patterns

This chapter presents the modeling, control, and simulation of hybrid electric vehicles for known daily commuting driving patterns. This chapter is organized as follows. Section 2.1 introduces the features of the approach. Section 2.2 presents the modeling and control for the 1 degree of freedom model. Section 2.3 provides the simulation results for known daily commuting driving patterns. Section 2.4 presents the discussion.

2.1 Features of the approach for known daily commuting driving patterns

There are three new features of the nonlinear real-time optimal control approach in the hybrid electric vehicle for known driving patterns.

First, the apparent relationship between the battery power and the future road load is addressed in the cost function of the fuel economy optimal control problem with a simplified HEV energy management system model. The fixed vehicle speed pattern can be predicted.

The battery charge can be adapted to the future road load to find better engine operating points and regenerate more free braking energy.

Second, the battery SOC constraint can be considered in advance in the nonlinear real-time optimal control approach. The nonlinear real-time optimal control approach has the advantage for dealing with constraints in a predictive control structure.

Third, it examines quantitatively the effects of operating the engine at the best efficiency operating points of the engine with a continuously variable transmission using a commercially available HEV hybrid electric vehicle energy management electronic control unit simulator. The power-split architecture addressed in this work can regulate engine operating points near it best efficient line.

The engine dynamics affects fuel consumption, therefore the engine dynamics needs to be considered for accuracy. Since the system may become too complex, an approach neglecting the engine dynamics is presented. When the controller is designed, it is assumed that the engine dynamics is neglected compared to the much slower dynamics of the battery [7]. As for the fuel consumption verification, the GT-SUITE engine model is used; the engine dynamics is not neglected. The GT-SUITE engine model contains the cam valve, thermo, intake air, throttle valve, exhaust gas dynamics.

2.2 Modeling and control for the 1 degree of freedom model

A conceptual diagram of the hybrid electric vehicle model is shown in Fig. 2.2.1. The driving condition is a driving pattern of three weeks based on real driving from Honda R&D

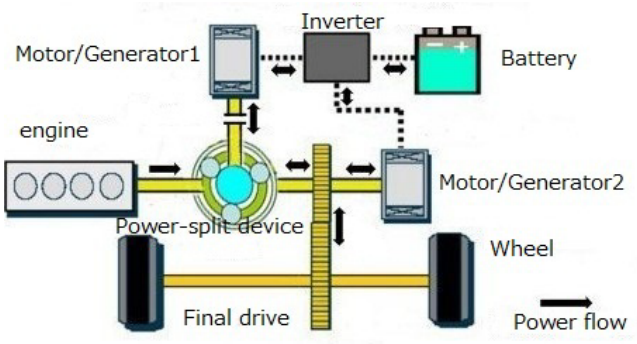

Figure 2.2.1: Model of the hybrid electric vehicle. Diagram adapted from [9]

Company to the employee's house. The design specifications require that driver's satisfaction parameter that is a function of the difference between the required vehicle speed and the real speed is above 90%. The HEV in this study has the power-split device which has both functionality of a speed coupler and CVT. There are five dynamic components: the engine, the battery, two motor/generators (M/Gs), and the wheels in this power-split HEV system. The MG1 is utilized to shift engine operating points to the engine best efficiency line during various road loads.

Since the battery dynamics is the slowest in the power plant, the dynamics of other components in the power plant can be neglected, the system dynamics is dominated by the battery dynamics. Therefore the system dynamics can be reduced to the battery dynamics. This can simplify the energy management scheme. This approach can also be seen in [7]. This simplification is possible because four constraints are introduced : the road load; the torque and speed relation of the speed coupler; the power flow relation among the five dynamic components; and the engine optimal operating line (OOL) using CVT. The power plant dynamics can be decomposed to the slow dynamics of the battery model, and the quick dynamics of the engine model and M/G model.

The property of the power-split device, which reveals the torque and speed relationships among the engine, M/Gs, and the road load, can be expressed as follows [92]:

$$\begin{aligned}\tau_{\text{eng}}(t) &= -(1+\frac{R}{S})\tau_{\text{M/G1}}(t) \\ &= -(1+\frac{S}{R})(\tau_{\text{M/G2}}(t) - \frac{\tau_{\text{req}}(t)}{g_{\text{f}}}) \\ S\omega_{\text{M/G1}}(t) &+ R\omega_{\text{M/G2}}(t) - (S+R)\omega_{\text{eng}}(t) = 0 \end{aligned} \tag{2.2.1}$$

where S and R are the number of the sun gear and the ring gear teeth, respectively; $\tau_{\text{M/G1}}$, $\tau_{\text{M/G2}}$, τ_{req}, and τ_{eng} are the torque of M/G1, M/G2, the road load, and the engine, respectively; $\omega_{\text{M/G1}}$, $\omega_{\text{M/G2}}$, and ω_{eng} are the angular velocities of M/G1, M/G2, and the engine, respectively; and g_{f} is the final drive gear ratio.

The power flow relationships among the five dynamic components at the inverter and the power-split device are given as

$$\begin{aligned} P_{\text{batt}}(t) &= P_{\text{M/G1}}(t) + P_{\text{M/G2}}(t) \\ P_{\text{req}}(t) &= P_{\text{M/G1}}(t) + P_{\text{M/G2}}(t) + P_{\text{eng}}(t) \end{aligned} \tag{2.2.2}$$

where P_{batt}, $P_{\text{M/G1}}$, $P_{\text{M/G2}}$, P_{eng}, and P_{req} are the power of the battery, M/G1, M/G2, the engine, and the road load, respectively.

The engine is assumed to work always along its OOL using CVT which can also be considered as a constraint. When the engine power is known, by looking up the table of OOL, the engine optimal speed and torque can be obtained.

The fuel consumption is approximated using the Willan's line method to reduce the complexity of the engine fuel consumption model. The HEV configuration in this work

can realize idle stop using the electric CVT. It was found that a good approximation was obtained using the Willan's line method [93]. The fuel consumption rate can be expressed as

$$\dot{m}_f(t) = c_f(P_{req}(t) - P_{batt}(t))/(1 + e^{-\beta(P_{req}(t)-P_{batt}(t))}) \tag{2.2.3}$$

where c_f is a constant. The parameter β decides the shape of the sigmoid function. The sigmoid function is chosen to evaluate the fuel consumption in case of making the vehicle slow down. So the vehicle is near to fuel cut when it slows down. The detailed explanation of this fuel consumption model is included in Appendix A.

The road load is known when the vehicle speed pattern is fixed. From the configuration of the power-split HEV system, the M/G2 speed is also known as

$$\omega_{\mathrm{M/G2}}(t) = \frac{g_{\mathrm{f}}}{r_{\mathrm{w}}} v_{\mathrm{req}}(t) \tag{2.2.4}$$

where r_{w} is the wheel radius; and v_{req} is the required vehicle speed by the driving speed pattern. This driving cycle required vehicle speed is the desired value of the nonlinear real-time optimal controller.

When the driving speed pattern is fixed, the engine and motor/generator dynamics can be neglected, therefore the system dynamics is reduced to the battery dynamics. The only optimization objective is the vehicle fuel economy. The only state variable is the battery SOC, x_{SOC}, and the control input is the battery power. The nonlinear battery model can be

described as follows [35]:

$$\begin{aligned} &\dot{x}(t) = f(u(t)) \quad x(t) = x_{\mathrm{SOC}}(t) \quad u(t) = P_{\mathrm{batt}}(t) \\ &f(u(t)) = -\frac{V_{\mathrm{OC}} - \sqrt{V_{\mathrm{OC}}^2 - 4P_{\mathrm{batt}}(t)R_{\mathrm{batt}}}}{2R_{\mathrm{batt}}Q_{\mathrm{batt}}} \end{aligned} \tag{2.2.5}$$

where x and u are the state and the control input, and V_{OC}, R_{batt}, and Q_{batt} are the battery open circuit voltage, the battery internal resistance, and the battery capacity, respectively. As stated in [35], in general, the SOC range of the battery usage is limited between 0.2 and 0.9, but in charge-sustaining problems, the battery mainly operates in a narrower range, e.g. from 0.5 to 0.7; hence, the voltage and the resistance may not vary so much in the range.

Since an approximate continuous and differentiable mathematical engine model is needed for the real-time optimal control algorithm, the linear engine model is used as above. However, as for the fuel economy evaluation in the ultimate simulation, the high fidelity engine model which is a lookup table that provides the engine fuel rate and efficiency as a function of instantaneous engine speed and engine torque is used. The other components of the HEV system like the CVT, the power electronics, the two motor/generators are modelled as a lot of lookup tables considering component efficiency in the benchmark simulator HEV model. These lookup tables are measured in a test bench. The approximate models of the engine and the battery for optimal control are used to integrate with the high fidelity models in the benchmark simulator HEV model.

The simplified modeling method is derived from the power relationships among the engine, the battery, and the road load. Since these relationships are general in an HEV configuration, this modeling approach explained above can be applied to other HEV configurations.

The optimal controller is divided into two levels. The high-level controller finds the

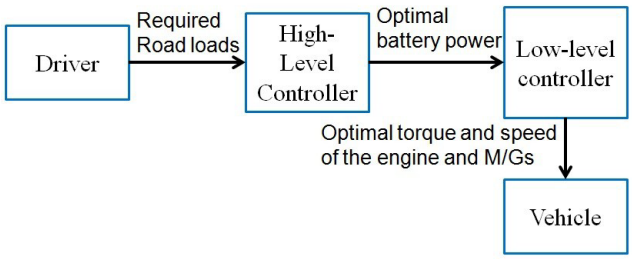

Figure 2.2.2: The proposed HEV energy management approach

optimal battery power, and the low-level controller determines the optimal torque and speed of the engine and the motor/generators (see Fig. 2.2.2).

The optimal control problem is formulated as

$$\text{Minimize: } J = \frac{1}{2}(x_{SOC} - x_f(t+T))^T S_f(x_{SOC} - x_f(t+T))$$
$$+ \int_t^{t+T} L(x_{\text{SOC}}(\tau|t), P_{\text{batt}}(\tau|t))d\tau \tag{2.2.6}$$
$$\text{Subject to: } P_{\text{battmin}} \leq P_{\text{batt}}(\tau|t) \leq P_{\text{battmax}} \tag{2.2.7}$$

where T is the prediction horizon; x_{f} is the desired final state value; and P_{battmin} and P_{battmax} denote the minimum battery power and the maximum battery power.

The objective of this optimal control problem is to minimize the fuel consumption, while the battery SOC is maintained between the thresholds. This is achieved by minimizing the cost function L, which includes four terms: the fuel consumption, the engine use and the mechanical brake use, the deviation of battery SOC from the reference value, and the

penalization of state constraint violations. The cost function L is defined as follows:

$$\begin{aligned} L &= w_1 c_{\mathrm{f}}(P_{\mathrm{req}} - P_{\mathrm{batt}})/(1 + e^{-\beta(P_{\mathrm{req}} - P_{\mathrm{batt}})}) \\ &+ w_2(P_{\mathrm{req}} - P_{\mathrm{batt}})^2 + w_3 \left(\frac{1}{2}(x_{\mathrm{SOC}} - SOC_{\mathrm{d}})\right)^2 \\ &+ w_4(-\ln(x_{\mathrm{SOC}} - SOC_{\mathrm{min}}) - \ln(SOC_{\mathrm{max}} - x_{\mathrm{SOC}})) \end{aligned} \tag{2.2.8}$$

where SOC_{d} is the desired battery SOC value; w_1, w_2, w_3 and w_4 are the weights; SOC_{min} and SOC_{max} denote the minimum battery SOC and the maximum battery SOC. The log barrier function is introduced as a penalizing term for violations of state constraints which are hard to be dealt with. The performance index value becomes very large when the state constraint is being violated. By doing so, the state constraint of the nonlinear system is satisfied automatically.

The two terms containing $P_{req} - P_{batt}$ have different roles. The first $P_{req} - P_{batt}$ term is for fuel economy evaluation using the Willan's line method. The sigmoid function in the term will lead the fuel consumption to 0 when the vehicle slows down. Since the motor/generator is much more efficient than the engine, the quadratic penalty $P_{req} - P_{batt}$ term is introduced to make best use of the battery energy and avoid using engine power.

Since the future road load is known a priori, the authors believe that it is natural and simple to adapt the battery power to the future road load to obtain better fuel economy. This relationship is clearly formulized as the second term of the cost function of the optimal control problem. It can make best use of the battery energy buffer. The battery can assist the vehicle driving during the acceleration process, and recuperate the free brake energy during the deceleration process. The engine operating points can also be shift to the engine OOL by this adaption.

At each time t, the optimal control input is computed by solving the above optimal control problem during the prediction horizon T. Only the first element of the optimal control sequence is applied. At the next time step, the prediction horizon moves forward and the process is repeated [95].

2.3 Computer simulation results of the nonlinear real-time optimal control algorithm with daily commuting driving patterns for HEVs

Effectiveness of the above proposed approach is validated by the benchmark simulator, which was provided by the Technical Committee on Automotive Control and Model Research (JSAE and SICE Joint) in SIMULINK® and GT-SUITE® [89]. The GT-SUITE engine model which contains the cam valve, thermo, intake air, throttle valve, exhaust gas dynamics has high fidelity. The fuel economy verification uses the GT-SUITE high fidelity engine model. In this simulation, vehicle parameters are obtained from the benchmark simulator. Fig. 2.3.1 gives the engine OOL of the HEV system. The driving condition is a driving pattern of three weeks based on real driving from Honda R&D Company to the employee's house. The total simulation time is 80456 [s] by the three week HEV driving patterns. The sampling time h is 0.01 [s]. The vehicle parameters are m=1460 [kg], ρ=1.23 [kg/m^3], $C_{\rm D}$=0.33, A=1.746 [m^2], g=9.8 [m/s^2], μ=0.015, $V_{\rm OC}$=201.6 [V], $R_{\rm batt}$=0.3192 [Ω] and $Q_{\rm batt}$=6.5 [Ah], $c_{\rm f}$=0.076. The control parameters are β=0.5, $SOC_{\rm d}$=0.6, $SOC_{\rm min}$=0.5, $SOC_{\rm max}$=0.7, $P_{\rm battmin}$=$-$20 [kW], $P_{\rm battmax}$=20 [kW], $x_{\rm f}$=0.6, $S_{\rm f}$=5×10^{11}, w_1=920, w_2=5×10^4, w_3=3.5×10^5, and w_4=0.001. The nonlinear real-time optimal control problem is solved

using the numerical computation method: the continuation and generalized minimum residual (C/GMRES) method [96]. A brief description of the solution of the proposed nonlinear real-time optimal control problem is included in Appendix B. The C/GMRES method uses forward difference approach (shown below), and discretizes the HEV plant with a sampling interval h to implement the nonlinear real-time optimal control algorithm.

$$\frac{dx}{d\tau} \approx \frac{x(t+\tau) - x(t)}{\tau}. \tag{2.3.1}$$

The rule-based control for HEVs introduces a set of rules to decide the power split between the engine and the battery after the vehicle states are observed. The benchmark problem rule-based control approach is used as a comparison for the proposed nonlinear real-time optimal control approach. The nonlinear real-time optimal control algorithm is realized by utilizing the C MEX S-function builder in MATLAB/SIMULINK. First, the optimal battery power is calculated by the high-level controller. Next, this optimal value is fed into the low-level controller where the optimal torque and speed of the engine and M/Gs are determined. Finally, these actual control input signals are applied to the commercially available Toyota Prius HEV energy management ECU simulator. The fuel economy is calculated using the benchmark simulator which is based on the GT-SUITE high fidelity HEV model.

Fig. 2.3.2 shows the simulation results of the benchmark problem rule-based approach. The battery SOC constraint is violated at about 30000 [s] of the simulation. Fig. 2.3.3 shows the simulation results of the nonlinear real-time optimal control approach. The battery SOC constraint is satisfied during the whole 80456 [s] simulation. In addition, the power of the engine and M/Gs are reasonable according to the commercially available Toyota Prius HEV energy management ECU.

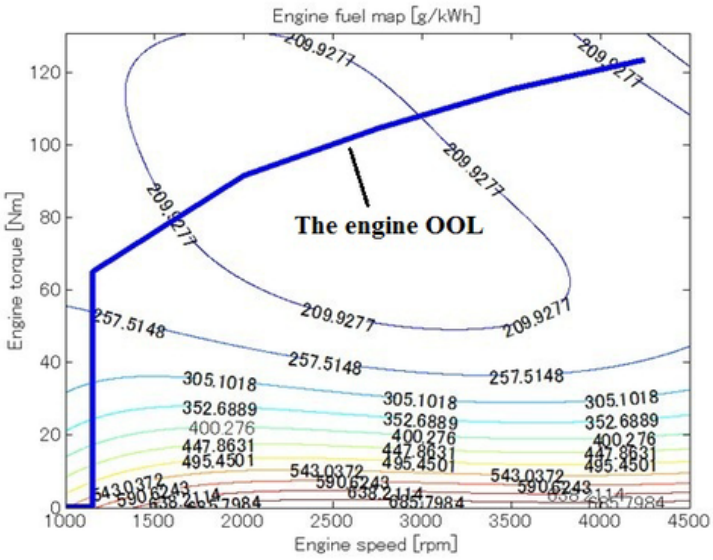

Figure 2.3.1: The engine OOL of the HEV system

A significant benefit of the power-split architecture is the fact that it decouples the engine crankshaft from the road, and allows the electric machines to move the engine speed where fuel efficiency is maximized [97]. This is identified by the engine operating points distribution in Fig. 2.3.4 and Fig. 2.3.5. As shown in Fig. 2.3.5 the nonlinear real-time optimal control approach operates the engine at fairly low speed and high torque, which means high engine efficiency and low brake specific fuel consumption values. The nonlinear real-time optimal control approach forces the engine to work regularly, above and close to the engine OOL. In contrast, the benchmark problem rule-based approach operates the engine at fairly high speed and low torque, which means low engine efficiency and high brake specific fuel consumption values. By adapting the battery power to the future road load, the nonlinear real-time optimal control approach develops the ability of the power-split architecture to shift the engine operating points to the engine OOL.

The detailed power-split characteristics of the benchmark problem rule-based approach

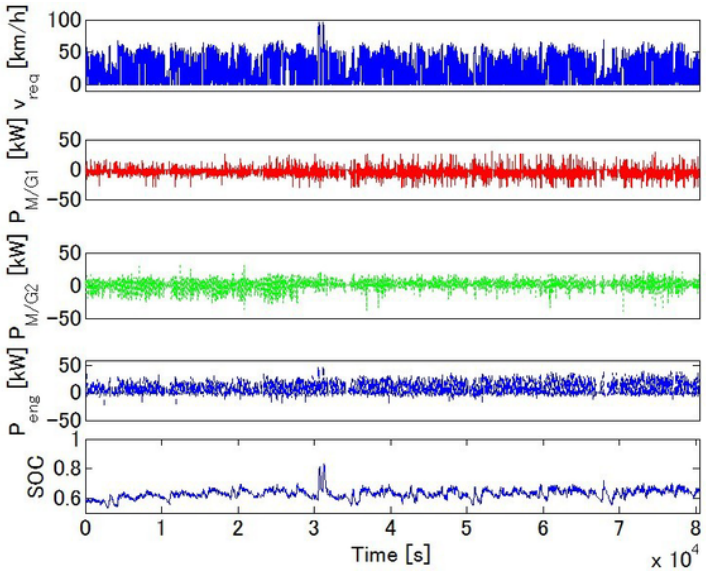

Figure 2.3.2: Simulation results of the benchmark problem rule-based approach

and the nonlinear real-time optimal control approach is shown in Fig. 2.3.6 and Fig. 2.3.7. As shown in Fig. 2.3.6, the benchmark problem rule-based approach cannot split the power properly according to the future road load. In contrast, the nonlinear real-time optimal control approach assists the engine when significant power is requested from the road load, recuperates the free regenerative braking energy during the deceleration period, and runs the HEV in all-electric mode during the cruise period. All of these lead to the improvement of the fuel efficiency by making best use of the battery energy buffer.

Table 2.3.1 presents the overall fuel economy comparison results. The initial battery SOC of all the cases is 0.6. The final battery SOC of the benchmark problem rule-based approach is 0.653. The final battery SOC of the nonlinear real-time optimal control approach is 0.654. Driver's satisfaction parameter is 100% in all the cases. We can see that the nonlinear real-time optimal control approach can improve fuel economy by 34.6% compared to the benchmark problem rule-based approach. The proposed vehicle tracking nonlinear

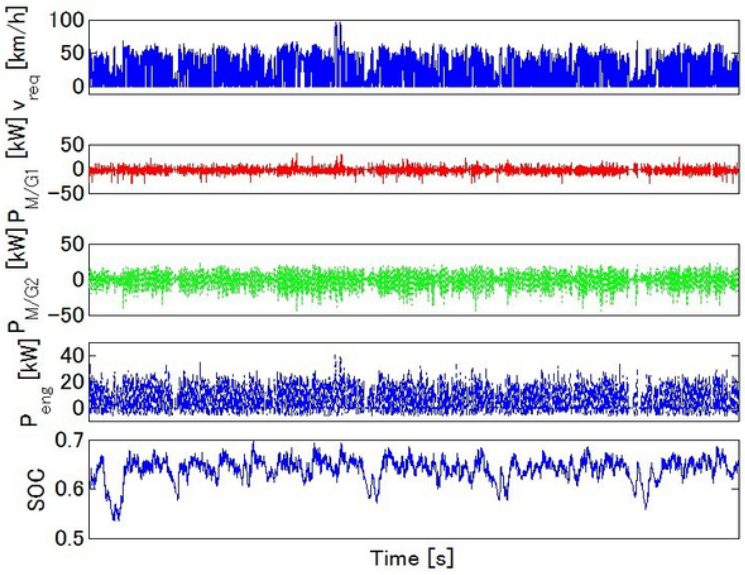

Figure 2.3.3: Simulation results of the nonlinear real-time optimal control approach

real-time optimal control algorithm is fast for computation. The simulation is run in a Matlab/Simulink environment using a laptop with an Intel processor at 2.27 [GHz] processing speed and 2 [GB] of RAM. The sampling interval is 10 [ms]. From Table 2.3.1, it is concluded that the proposed vehicle tracking nonlinear real-time optimal control algorithm has the potential for real-time vehicle control. A shorter prediction horizon leads to less computational complexity and computation time. Since the battery dynamics is very slow, there are not many fuel economy improvements when a longer prediction horizon is considered. However, the short prediction horizon is enough for predicting future vehicle acceleration/deceleration to prepare the battery for discharging/charging. The nonlinear real-time optimal control approach can keep the final battery SOC above the initial battery SOC, which is important to the HEV charge sustainability. These results are promising because the fuel economy is calculated by GT-SUITE high fidelity HEV model of a real engine, which is the most accurate evaluation method in the computer simulation environment.

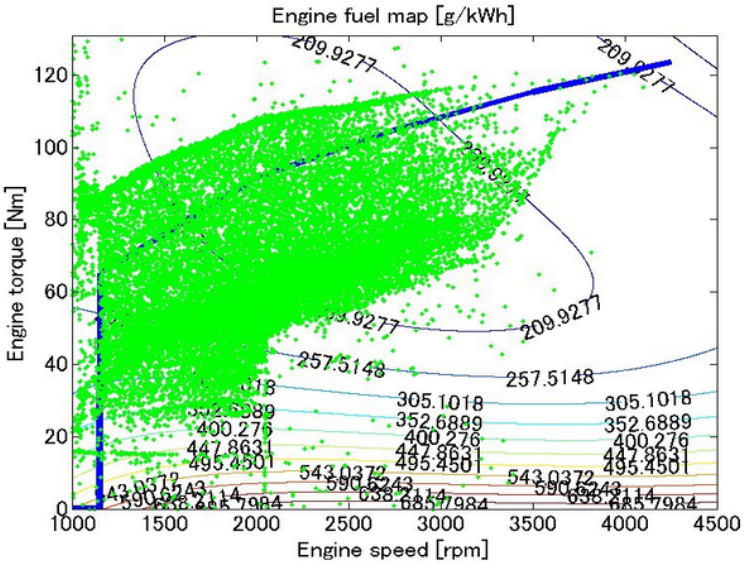

Figure 2.3.4: Engine operating point distribution using the benchmark problem rule-based approach

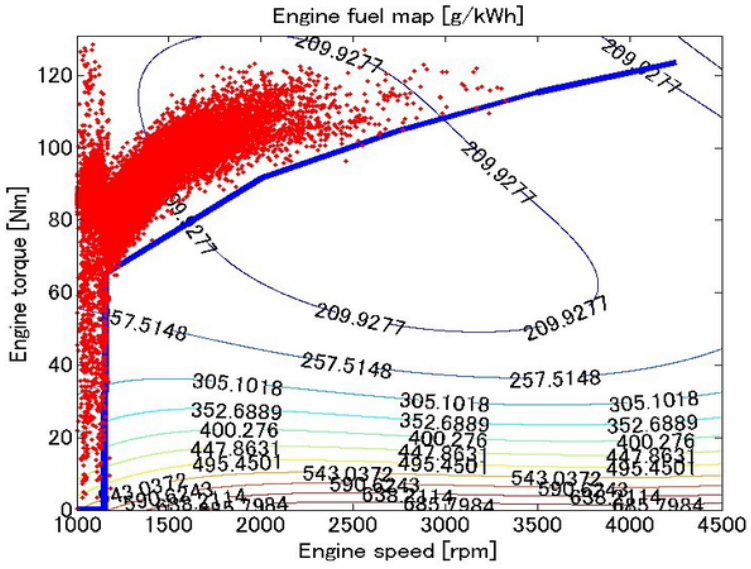

Figure 2.3.5: Engine operating point distribution using the nonlinear real-time optimal control approach

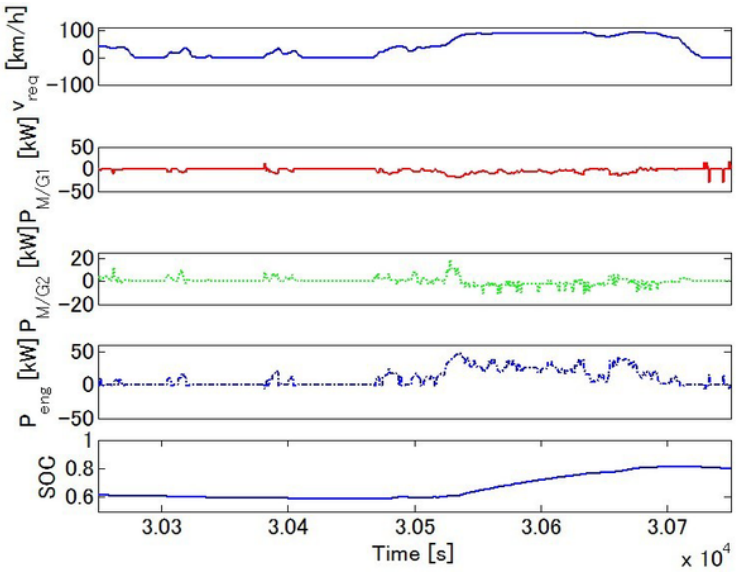

Figure 2.3.6: Detailed simulation results of the benchmark problem rule-based approach

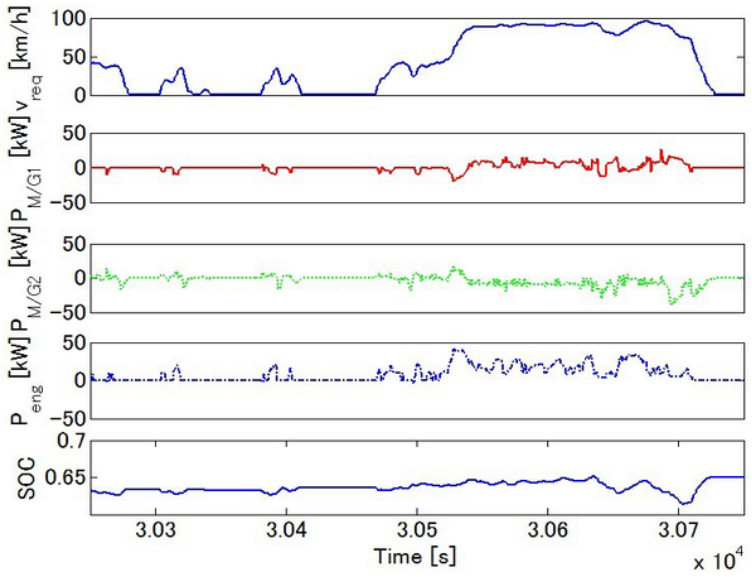

Figure 2.3.7: Detailed simulation results of the nonlinear real-time optimal control approach

Table 2.3.1: Fuel economy comparison results for daily commuting driving patterns, where T is the prediction horizon, ACT represents average computation time per sampling interval, and MCT represents max computation time per sampling interval.

Method	T [s]	ACT [s]	MCT [s]	Fuel economy [km/l]
Proposed method	0.01	7.7×10^{-5}	0.012	25.17(+34.5%)
Proposed method	0.02	8.5×10^{-5}	0.013	25.18(+34.6%)
Proposed method	0.1	1.9×10^{-4}	0.012	25.17(+34.5%)
Proposed method	1	0.014	0.045	25.18(+34.6%)
Proposed method	5	0.0064	0.046	25.17(+34.5%)
Proposed method	10	0.0125	0.06	25.18(+34.6%)
Benchmark	-	-	-	18.71

2.4 Discussion for the simulation with known daily commuting driving pattern

Since the engine and motor/generators dynamics is assumed to be neglectable, the proposed controller calculates the optimal power of the engine and motor/generators as manipulating variables. Ordinarily, the inertia of the engine is not negligible. In the fuel economy verification, the engine inertia is considered using the GT-SUITE high fidelity engine model. From the engine operating point distribution using the proposed approach, it is shown that the engine operating points deviate from the engine optimal operating line because of the delay of the engine. However in the real-time optimal controller, in order to reduce the computation cost, the dynamics of the engine is neglected.

After the optimal battery power is determined by the optimal control algorithm, the engine power can be decided. When the engine power is known, by looking up the table of OOL in the low-level controller, the engine optimal speed and torque reference values can be obtained. The real-time optimal control approach which can use future information can

improve the track ability compared with ordinary feedback control.

CHAPTER III

Driving cycle and engine operating point optimization for unknown driving patterns

This chapter presents the modeling, control, and simulation of hybrid electric vehicles for unknown driving patterns with slope and traffic information. This chapter is organized as follows. Section 2.1 introduces the features of the approach. Section 2.2 presents the modeling and control for the 3 degrees of freedom model. Section 2.3 provides the simulation results for the unknown driving pattern with slope information. Section 2.4 provides the simulation results for the unknown driving pattern with slope and traffic information. Section 2.5 presents the discussion.

3.1 Features of the approach for unknown driving patterns

There are five new features of the nonlinear real-time optimal control approach in the hybrid electric vehicle for unknown driving patterns.

First, both the driving cycle profile and the engine operating point are optimized using the approach.

Second, considering the HEV physical constraints like the speed and torque limits of the engine and motor/generators, and the battery state of charge beforehand makes the optimization and the fuel improvements trustworthy. The nonlinear real-time optimal control approach can consider constraints in real-time.

Third, the performance index can be systematically designed. The controller is constructed considering just the control objectives and the system constraints which is a nature and causal design process. This systematic design process can be applicable to other fuel optimization problems for HEVs and PHEVs.

Fourth, the proposed method gives the freedom of vehicle spacing between the preceding vehicle and the host vehicle. The vehicle spacing is kept above the minimum value, and this gives the freedom of control for vehicle speed variety to get battery fuel economy. This freedom can be obtained by the real-time optimal control.

Fifth, using the HEV property, the desired battery state of charge is designed according to the road slopes for better recuperation of free braking energy. It is not good for the HEV fuel economy if the HEV reaches the top of a hill with a fully charged battery. It is difficult to obtain the desired battery state of charge profile from the optimization view. The fuel

economy is improved due to this desired battery state of charge adaption.

In [98]- [100], the authors stated that the conventional engine optimal operating line idea is valid only if the power transmission loss is negligible or if it shows only a mild change throughout the operation condition. However, HEVs have far more complicated and irregular power transmission mechanisms and characteristics than conventional vehicles do. This complexity is mainly due to the electrical power transmission paths which involve non-linear power conversion losses in M/Gs. In other words, HEVs have an energy buffer like batteries whose efficiency is highly nonlinear to the input road loads. The battery can utilize the free regenerative braking energy to improve fuel economy significantly. The engine optimal operation for HEVs corresponding to the system optimality needs to be reconsidered. The engine and the motor/generator dynamics is considered for accuracy and global optimality instead of operating the engine near its optimal operating line.

3.2 Modeling and control for the 3 degrees of freedom model

The power-split device property which reveals the torque and speed relationships among the engine, M/Gs, and the road load can be expressed as follows [92], [9]:

$$
\begin{aligned}
& I_{M/G1}\dot{\omega}_{M/G1} = \tau_{M/G1} + fS \\
& (I_{M/G2} + \frac{I_w}{g_f^2} + m\frac{r_w^2}{g_f^2})\dot{\omega}_{M/G2} = \tau_{M/G2} - \frac{\tau_{resist} + \tau_{brake}}{g_f} + fR \\
& I_{eng}\dot{\omega}_{eng} = \tau_{eng} - f(R+S) \qquad (3.2.1) \\
& \tau_{resist} = r_w mg(\mu\cos(\theta) + \sin(\theta)) + \frac{1}{2}\rho C_D A r_w v^2 \qquad (3.2.2)
\end{aligned}
$$

where S and R are the number of the sun gear and the ring gear teeth, respectively; $\tau_{M/G1}$, $\tau_{M/G2}$, τ_{resist}, τ_{brake}, and τ_{eng} are the torque of M/G1, M/G2, the vehicle resistance, the friction brake, and the engine, respectively; $\omega_{M/G1}$, $\omega_{M/G2}$ and ω_{eng} are the angular velocities of M/G1, M/G2, and the engine, respectively; g_f is the final drive gear ratio; v is the vehicle speed; $I_{M/G1}$, $I_{M/G2}$, I_w, and I_{eng} are the inertia of M/G1, M/G2, the wheels, and the engine, respectively; r_w is the wheel radius; f is the internal force of the power-split device on the pinion gears; ρ, C_D, A, m, g, μ and θ are the air density, the air drag coefficient, the frontal area of the vehicle, the vehicle mass, the gravity acceleration, the rolling resistance coefficient, and the road grade, respectively.

The relationships among the speed of the powertrain components are given as

$$S\omega_{M/G1} + R\omega_{M/G2} - (S+R)\omega_{eng} = 0 \tag{3.2.3}$$

$$\omega_{M/G2} = \frac{g_f}{r_w} v. \tag{3.2.4}$$

The power-balancing constraint needs to be considered. Since the power is a multiplication of the toque and the speed, the torque balance is presented in Equation (3.2.1), the power-balancing constraint is addressed identically. The power-balancing can is implicitly considered.

Using (3.2.1), (3.2.3), and (3.2.4) and eliminating the internal force f, the dynamics of

the engine and M/G2 is obtained:

$$\begin{bmatrix} I_{eng} + \left(\frac{S+R}{S}\right)^2 I_{M/G1} & -\frac{R(S+R)}{S^2} I_{M/G1} \\ -\frac{R(S+R)}{S^2} I_{M/G1} & I_{M/G2} + \frac{I_w}{g_f^2} + \left(\frac{R}{S}\right)^2 I_{M/G1} + m\frac{r_w^2}{g_f^2} \end{bmatrix} \begin{bmatrix} \dot{\omega}_{eng} \\ \dot{\omega}_{M/G2} \end{bmatrix} = \begin{bmatrix} \tau_{eng} + \frac{S+R}{S}\tau_{M/G1} \\ \tau_{M/G2} - \frac{R}{S}\tau_{M/G1} - \frac{\tau_{resist}+\tau_{brake}}{g_f} \end{bmatrix}. \tag{3.2.5}$$

The fuel consumption rate is evaluated using the Willan's line method [101]. It uses the function of the engine speed and torque to approximate the engine fuel consumption rate map directly, which leads to more accurate results than those of polynomial approximations. The fuel consumption rate can be expressed as follows [102]:

$$\dot{m}_f = \frac{a\tau_{eng}\omega_{eng} + b\omega_{eng} + c\omega_{eng}^3}{h + k\omega_{eng} + l\omega_{eng}^2} \tag{3.2.6}$$

where $\dot{m}_f$ is the fuel consumption rate; a, b, c, h, k, and l are constant parameters.

Based on the previous analysis, the system dynamics is reduced to the battery dynamics, the engine dynamics, and the vehicle dynamics. The nonlinear system model is then

represented by

$$
\begin{aligned}
&\dot{x} = f(x,u)\\
&x = \begin{bmatrix} \omega_{eng} \; p \; \omega_{M/G2} \; x_{SOC} \end{bmatrix}^T\\
&u = \begin{bmatrix} \tau_{eng} \; \tau_{M/G2} \; \tau_{M/G1} \; \tau_{brake} \end{bmatrix}^T\\
&f(x,u) =\\
&\begin{bmatrix}
M\tau_{eng} + N\tau_{M/G2} + (M\frac{S+R}{S} - N\frac{R}{S})\tau_{M/G1} - N\frac{\tau_{resist}+\tau_{brake}}{g_f}\\
\frac{r_w}{g_f}\omega_{M/G2}\\
N\tau_{eng} + P\tau_{M/G2} + (N\frac{S+R}{S} - P\frac{R}{S})\tau_{M/G1} - P\frac{\tau_{resist}+\tau_{brake}}{g_f}\\
-\frac{V_{OC}-\sqrt{V_{OC}^2-4P_{batt}R_{batt}}}{2R_{batt}Q_{batt}}
\end{bmatrix}\\
&\begin{bmatrix} M & N \\ N & P \end{bmatrix} =\\
&\begin{bmatrix}
I_{eng} + \left(\frac{S+R}{S}\right)^2 I_{M/G1} & -\frac{R(S+R)}{S^2} I_{M/G1}\\
-\frac{R(S+R)}{S^2} I_{M/G1} & I_{M/G2} + \frac{I_w}{g_f^2} + \left(\frac{R}{S}\right)^2 I_{M/G1} + m\frac{r_w^2}{g_f^2}
\end{bmatrix}^{-1}
\end{aligned}
\tag{3.2.7}
$$

where p is the vehicle position. x_{SOC} is the battery SOC; V_{OC}, R_{batt}, and Q_{batt} are the battery open circuit voltage, the battery internal resistance, and the battery capacity, respectively; and M, N, and $P \in \mathbb{R}$. We use the vehicle position and the vehicle speed to represent the vehicle dynamics. The battery power P_{batt} is governed by

$$
P_{batt} = \tau_{M/G1}\omega_{M/G1}\eta_{M/G1}^n + \tau_{M/G2}\omega_{M/G2}\eta_{M/G1}^n. \tag{3.2.8}
$$

where $\eta_{M/G1}$ and $\eta_{M/G2}$ are the average efficiency of M/G1 and M/G2, and

$$n = \begin{cases} 1, & \text{if generating} \\ -1, & \text{if motoring.} \end{cases} \tag{3.2.9}$$

The nonlinear model of the power-split HEV with slope information includes the vehicle speed dynamics. The vehicle speed profile can be optimized with this nonlinear model.

The optimal control problem is defined as

$$\begin{aligned} \min_{u} J = \int_{t}^{t+T} L(x(\tau|t), u(\tau|t))d\tau \\ \text{subject to } \tau_{M/G2min} \leq \tau_{M/G2}(\tau|t) \leq \tau_{M/G2max} \\ \tau_{M/G1min} \leq \tau_{M/G1}(\tau|t) \leq \tau_{M/G1max} \\ 0 \leq \tau_{brake}(\tau|t) \leq \tau_{brakemax} \end{aligned} \tag{3.2.10}$$

where T is the prediction horizon; $\tau_{M/G2max}$, $\tau_{M/G2min}$, $\tau_{M/G1max}$, $\tau_{M/G1min}$, and $\tau_{brakemax}$ denote the bounds of the control inputs.

The following objectives are considered in this optimal control problem.

L_x: the fuel consumption is minimized.

L_y: the vehicle deceleration or acceleration is moderated.

L_z: the vehicle speed is kept near to its desired value.

L_d: the battery SOC is kept near to its desired value. This is one of the cores of the proposed approach. The battery energy is adapted to the vehicle future energy requirements by setting the desired battery SOC as a function of road slopes which represent the main

part of the future road load.

L_e: the battery SOC constraint is kept satisfied.

L_f: the engine speed constraint is kept satisfied.

L_g: the M/G2 speed constraint is kept satisfied.

L_h: the mechanical brake use is minimized.

L_i: the M/G1 speed constraint is kept satisfied.

L_j: the battery power constraint is kept satisfied.

L_k: the engine torque constraint is kept satisfied.

L_l: the following distance constraint is kept satisfied. This is also one of the cores of the proposed approach. The following distance constraint is kept in a predictive controller structure. The host vehicle maneuvers are independent of the preceding vehicle. The proposed approach does not require inter-vehicle communication. The following distance is changed above the minimum following distance, which improves the freedom of eco-driving car following control to optimize the driving profile for better fuel economy.

The cost function L is defined as follows:

$$
\begin{aligned}
L &= w_x L_x + w_y L_y + w_z L_z + w_d L_d + w_e L_e + w_f L_f \\
&+ w_g L_g + w_h L_h + w_i L_i + w_j L_j + w_k L_k + w_l L_l + w_m L_m \\
L_x &= \dot{m}_f \\
L_y &= \frac{1}{2}(\frac{r_w}{g_f}\dot{\omega}_{M/G2} + g\sin(\theta))^2 \\
L_z &= \frac{1}{2}(v - v_d)^2 \\
L_d &= \frac{1}{2}(x_{SOC} - SOC_d(p))^2 \\
L_e &= -\ln(x_{SOC} - SOC_{min}) - \ln(SOC_{max} - x_{SOC}) \\
L_f &= -\ln(\omega_{eng}) - \ln(\omega_{engmax} - \omega_{eng}) \\
L_g &= -\ln(\omega_{M/G2}) - \ln(\omega_{M/G2max} - \omega_{M/G2}) \\
L_h &= \frac{1}{2}(\tau_{brake})^2 \\
L_i &= -\ln(\omega_{M/G1} - \omega_{M/G1min}) - \ln(\omega_{M/G1max} - \omega_{M/G1}) \\
L_j &= -\ln(P_{batt} - P_{battmin}) - \ln(P_{battmax} - P_{batt}) \\
L_k &= -\ln(\tau_{eng}) - \ln(\tau_{engmax} - \tau_{eng}) \\
L_l &= -\ln(p_p(t) + v_p(t)(\tau - t) - p(t) - l_p - d_{min})
\end{aligned}
\tag{3.2.11}
$$

where $SOC_d(p)$ is the desired battery SOC value. The parameter v_d is the desired vehicle speed. It is chosen as the best constant speed fuel economy speed. The parameters w_x, w_y, w_z, w_d, w_e, w_f, w_g, w_h, w_i, w_j, w_k, w_l are the weights. The parameters SOC_{min}, SOC_{max}, ω_{engmax}, $\omega_{M/G2max}$, $\omega_{M/G1min}$, $\omega_{M/G1max}$, $P_{battmin}$, $P_{battmax}$, and τ_{engmax} denote the bounds of the parameters. The parameter τ_{engmax} is a state variant control input. It is a function of the engine speed. The parameters p_p, v_p, l_p, and d_{min} denote the preceding vehicle position,

the preceding vehicle speed, the preceding vehicle length, and the minimum vehicle spacing. The preceding vehicle speed in the prediction horizon is assumed to be constant, and its value is the same as the observed preceding vehicle speed at the beginning of the nonlinear real-time optimal control algorithm. In this way, the vehicle spacing can be kept above the minimum vehicle spacing in the prediction horizon.

The log barrier functions are introduced as penalizing terms for violations of the state constraints and the state variant control input constraint. The value of the performance index becomes very large when the constraints are being violated. By doing so, the state constraints and the state variant control input constraint of the system are satisfied. The general rule that the engine always works along its optimal operating line does not promise optimal fuel economy. Due to lack of future road load information, the engine may work in the low efficiency parts of the engine optimal operating line. The industrial tradition which assumes that the engine always works along its optimal operating line in the commercially available HEV energy management strategy is not followed. The fuel economy is optimized using the only term concerning the fuel consumption rate in the cost function. It will search the whole areas of the engine fuel consumption map for better fuel economy. In this way we want to develop the full strength of HEVs.

The inequality constraint in the optimal control problem is converted to an equality constraint by introducing a dummy input u_d for computation simplicity as follows:

$$C(x(t), u(t)) = u^2(t) + u_d^2(t) - u_{max}^2 = 0 \tag{3.2.12}$$

where u_{max} denotes the bound of the control input.

To solve this optimal control problem with the calculus of variation method [94], the

Hamiltonian function is defined by

$$H(x, u, \lambda, \psi) = L(x, u) + \lambda^T f(x, u) + \psi^T C(x, u) \tag{3.2.13}$$

where λ denotes the co-state, and ψ denotes the Lagrange multiplier associated with the equality constraint.

The first-order necessary conditions for the optimal control input u, the multiplier ψ, and the co-state λ are obtained using the calculus of variation as

$$\begin{aligned} &\dot{x} = f(x, u) \quad x(t_0) = x_0 \\ &\dot{\lambda} = -\frac{\partial H}{\partial x} \quad \lambda(t + T) = 0 \\ &\frac{\partial H}{\partial u} = 0 \\ &C(x, u) = 0 \end{aligned} \tag{3.2.14}$$

where t_0 is the initial time, and x_0 is the initial state.

The derivative of the co-state λ concerning the slope information and the battery SOC is obtained as

$$\begin{aligned} &\dot{\lambda}_2 = -\lambda_1 \frac{\partial \dot{\omega}_{eng}}{\partial p} - \lambda_3 \frac{\partial \dot{\omega}_{M/G2}}{\partial p} - w_y \frac{\partial L_y}{\partial p} - w_l \frac{\partial L_l}{\partial p} - w_d \frac{\partial L_d}{\partial p} \\ &\dot{\lambda}_4 = -w_d (x_{SOC} - SOC_d) \\ &-w_e \left(\frac{1}{SOC_{max} - x_{SOC}} - \frac{1}{x_{SOC} - SOC_{min}} \right). \end{aligned} \tag{3.2.15}$$

It reveals that the co-state of the vehicle position is related to the two power devices, the terms concerning the vehicle acceleration or deceleration, the desired battery SOC, and the

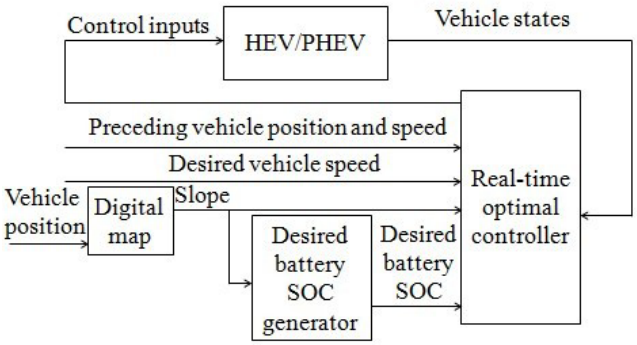

Figure 3.2.1: Structure of the nonlinear real-time optimal control system.

vehicle spacing in the cost function. The battery SOC co-state is affected by the battery desired SOC and the bounds of the battery SOC. A large co-state will lead to the small variation of the battery SOC. A small co-state will lead to the large variation of the battery SOC. A well tuned performance index and weights can lead to a better system.

The structure of the nonlinear real-time optimal control system is shown in Fig. 3.2.1. The system inputs contain the control inputs. The system outputs consist of the vehicle states. The preceding vehicle position and speed can be measured using digital maps and vehicle laser devices. The real-time optimal controller uses terrain information from digital maps to calculate $SOC_d(p)$ and $\theta(p)$. The energy management problem can be viewed as an optimal control problem which is addressed here using a nonlinear real-time optimal control approach.

3.3 Simulation results for the unknown driving pattern with slope information

In this simulation, vehicle parameters are used from ADVISOR 2002 [91]. The vehicle parameters are m=1504 [kg], ρ=1.23 [kg/m^3], C_{D}=0.3, A=1.746 [m^2], g=9.8 [m/s^2], μ=0.015, V_{OC}=307.85 [V], R_{batt}=1.004 [Ω], Q_{batt}=6 [Ah], r_{w}=0.287 [m], g_{f}=3.93, I_{eng}=0.18 [kgm^2], $I_{\mathrm{M/G1}}$=0.0226 [kgm^2], $I_{\mathrm{M/G2}}$=0.0226 [kgm^2], I_{w}=3.3807 [kgm^2], a=40.88, b=1576, c=$-$0.004051, h=1032000, k=365.7, l=$-$2.401, S=30, and R=78. The control parameters are T=10 [s], the sampling period h=0.1 [s], SOC_{d}=0.7, SOC_{min}=0.6, SOC_{max}=0.8, $\tau_{\mathrm{M/G2max}}$=305 [Nm], $\tau_{\mathrm{M/G2min}}$=$-$305 [Nm], $\tau_{\mathrm{M/G1max}}$=55 [Nm], $\tau_{\mathrm{M/G1min}}$=$-$55 [Nm], τ_{brakemax}=2655 [Nm], P_{battmin}=$-$23.684 [kW], P_{battmax}=23.684 [kW], v_{d}=60 [km/h], ω_{engmax}=418.8790 [rad/s], $\omega_{\mathrm{M/G2max}}$=628.3185 [rad/s], $\omega_{\mathrm{M/G1min}}$=$-$575.9587 [rad/s], $\omega_{\mathrm{M/G1max}}$=575.9587 [rad/s], w_{x}=42000, w_{y}=9000, w_{z}=800, w_{d}=30000000, w_{e}=120000, w_{f}=10000, w_{g}=50000, w_{h}=10, w_{i}=0.1, w_{j}=0.1, w_{k}=1000, and w_{l}=0. The optimal control problem is solved using the numerical computation method: the continuation and generalized minimum residual (C/GMRES) method [96]. The rule-based control for HEVs introduces a set of rules to decide the power split between the engine and the battery after the vehicle states are observed. The ADVISOR rule-based control approach is used as a comparison for the proposed approach. The driving pattern used in ADVISOR is obtained from the automatic speed control device (ASCD). ASCD is a kind of proportional-integral control method without slope previews. The real-time optimal control algorithm is realized by utilizing the C MEX S-function builder in Matlab/Simulink. Direct control input torque of the engine, the two M/Gs, and the mechanical brake are given by the real-time optimal controller. The fuel economy is calculated using the engine maps which are obtained from ADVISOR 2002. The simulation is con-

ducted using a typical up-down slope in Case 1 firstly, and then the results of a typical road of 6.2 [km] in Japan are observed in Case 2. The typical up-down slopes which have long and constant steep slopes are utilized to validate the full strength of the proposed approach. Since the prediction horizon cannot be lengthened enough for the battery dynamics, the desired battery SOC value is set according to the road elevation which represents the main part of the future road load information. It is reasonable to utilize the road elevation information since this future road load information is known already.

3.3.1 Case 1

The up slope of this road is 5% and the down slope of this road is -5%. The simulation results of Case 1 are presented in Fig. 3.3.1, Fig. 3.3.2, Fig. 3.3.3, and Fig. 3.3.4. Fig. 3.3.1 gives the comparison simulation results of the driving profile based on the proposed algorithm and the ASCD algorithm. The first column of Fig. 3.3.1 is the vehicle control input. The next two columns show the optimized vehicle speed and the road elevation. The real-time optimal control vehicle predicts the upcoming uphill and accelerates in advance to avoid the abrupt acceleration at the beginning of the uphill. The real-time optimal control vehicle can also predict the upcoming downhill and decelerate in advance to avoid the abrupt deceleration at the beginning of the downhill. In this way the proposed algorithm helps to improve the fuel economy.

Fig. 3.3.2 shows the power-split profile of the proposed algorithm. The desired battery SOC is assumed using the function as

$$SOC_{\mathrm{d}}(p) = 0.1\sin(\frac{\pi}{2000}p) + 0.695. \tag{3.3.1}$$

The columns of Fig. 3.3.2 from the top are the speed of the engine and the two M/Gs, the torque of the engine and the two M/Gs, the power of the engine and the two M/Gs, the battery SOC, and the road elevation. The real-time optimal control vehicle predicts the upcoming uphill and charges the battery in advance. When the vehicle comes to the uphill, the battery can assist the vehicle driving properly and reduce the battery SOC for the upcoming downhill charging. The battery is charged up during the downhill process using the energy recovered from the regenerative braking. By using the slope information in advance to better use the battery energy, the real-time optimal control algorithm helps to reduce the fuel consumption. Fig. 3.3.3 shows the power-split profile of the vehicle using the ADVISOR algorithm. We can see that without slope previews, the engine and the M/Gs work abruptly, especially at the beginning of the simulation; and the link parts of different slopes. The battery SOC decreases continually. The vehicle does not get the regenerative braking energy properly.

Fig. 3.3.4 shows the distribution of the engine operating points using the real-time optimal control algorithm and the ADVISOR algorithm. The crosses and the circles denote the engine operating points using the real-time optimal control algorithm and the ADVISOR algorithm, respectively. The line at the top left corner is the engine max torque line. The engine operating points cannot go beyond the line. We can see that the engine operating points of the real-time optimal control algorithm are distributed in better areas than those of the ADVISOR algorithm.

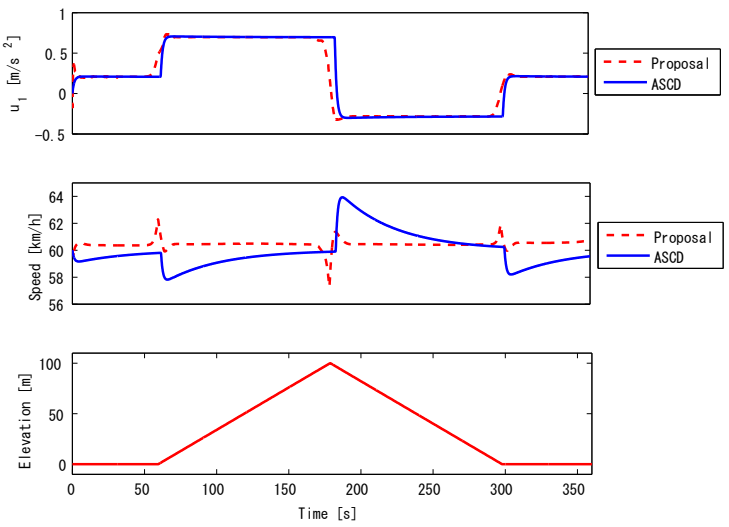

Figure 3.3.1: Driving profile of the real-time optimal control algorithm and the ASCD algorithm in Case 1.

3.3.2 Case 2

The effectiveness of the proposed energy management system of the power-split HEV is evaluated using the slope information of a real road. It is a road from the Imajuku traffic light position to the Hatae traffic light position which is 6.2 [km] located at Route 202, Fukuoka, Japan. The maximum slope of this road is 3.65% and the minimum slope of this road is -3.46%. Compared with the only big up-down slope in Case 1, there are a few small up-down slopes and a big up-down slope in Case 2. This real terrain is typical in Japan where there are many hilly areas.

The simulation results of Case 2 are presented in Fig. 3.3.5, Fig. 3.3.6, Fig. 3.3.7, and Fig. 3.3.8. Fig. 3.3.5 gives the comparison simulation results of the driving profile between the proposed algorithm and the ASCD algorithm. The proposed algorithm shows roughly the same control characteristics as those in Case 1. The real-time optimal control vehicle can

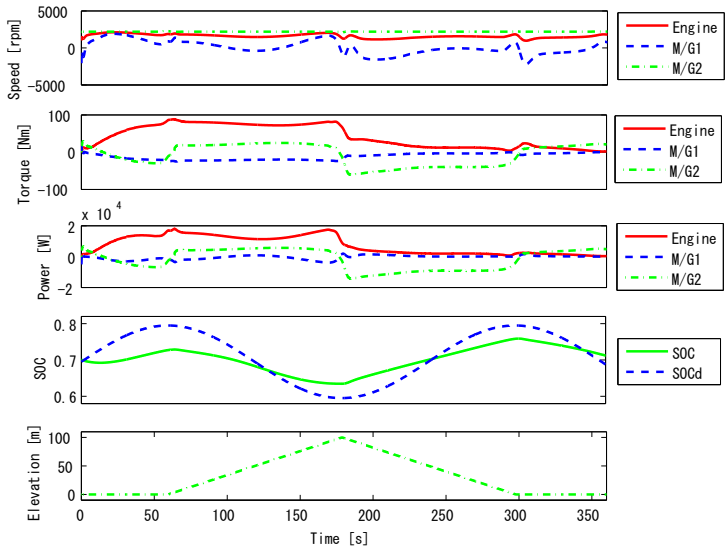

Figure 3.3.2: Power-split profile of the vehicle using the real-time optimal control algorithm in Case 1.

make good use of the predictive information of the road slopes and avoid abrupt accelerations and decelerations to get better fuel economy. The real-time optimal control vehicle can also utilize the advantage of the vehicle speed range, which can develop the possible energy saving ability of the HEV better. For example, it does not use the mechanical brake much to decelerate the vehicle during the downhill driving. A higher vehicle speed can produce larger regenerative braking energy.

Fig. 3.3.6 shows the power-split profile of the vehicle using the real-time optimal control algorithm. The desired battery SOC is assumed using the function as

$$SOC_{\mathrm{d}}(p) = -2.5\left(\frac{s_1}{1+e^{(}s_3(p-s_2))}+\frac{s_4}{1+e^{(}s_6(p-s_5))}+\cdots\right)+0.71. \tag{3.3.2}$$

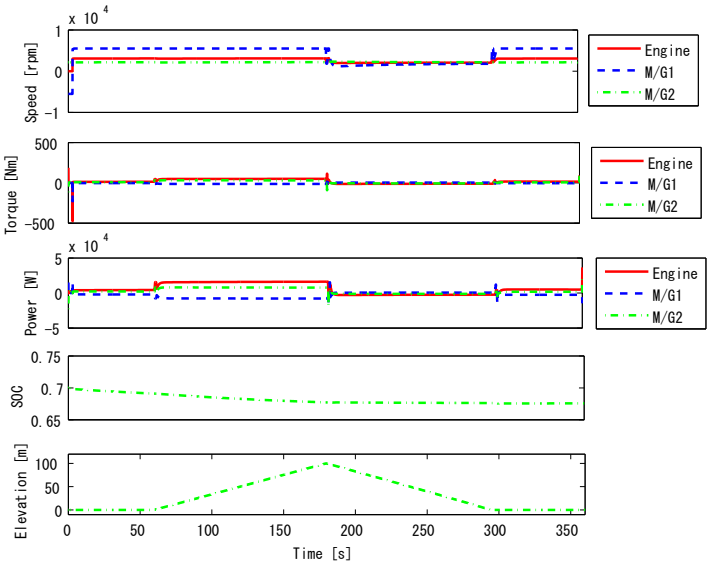

Figure 3.3.3: Power-split profile of the vehicle using the ADVISOR rule-based algorithm in Case 1.

The real-time optimal control vehicle performs roughly the same as that in Case 1. From Case 1 and Case 2 we can see that there is some causality between the road elevation and the battery SOC. The lowest point of the road elevation corresponds to the highest point of the battery SOC. The highest point of the road elevation corresponds to the lowest point of the battery SOC. By using the slope information in advance to better use the battery SOC range, the real-time optimal control algorithm helps to reduce the fuel consumption efficiently. Fig. 3.3.7 shows the power-split profile of the vehicle using the ADVISOR algorithm. The results can be explained in the same way as that in Case 1.

Fig. 3.3.8 shows the distribution of the engine operating points using the real-time optimal control algorithm and the ADVISOR rule-based algorithm. We can see from the results of Case 1 and Case 2 that the real-time optimal control algorithm can make the engine work in better areas rather than those along the best efficiency line of the engine

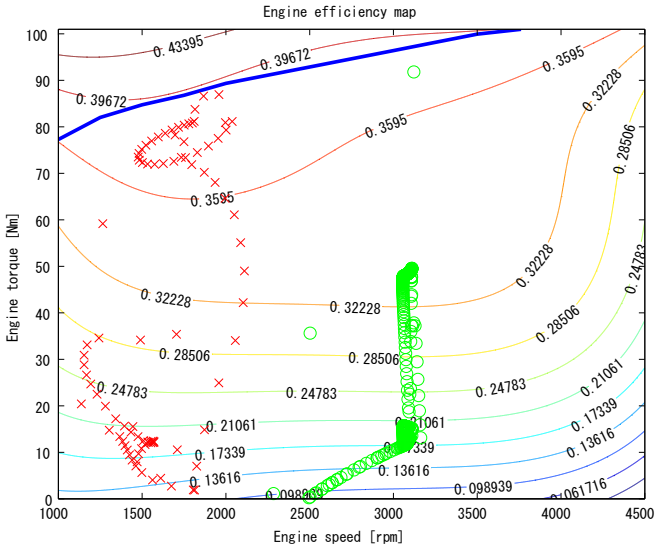

Figure 3.3.4: Engine operating point distribution using the real-time optimal control algorithm and the ADVISOR rule-based algorithm in Case 1.

using the CVT. Working along the best efficiency line of the engine does not promise best fuel efficiency. The fuel efficiency depends on the real efficiency of the engine, which makes the point that a high efficiency area is more profitable than the area near the engine OOL. We can see that better using of the battery SOC range results in better engine operating points.

The overall fuel economy results in the two cases are presented in Table 3.3.1. We can see that the real-time optimal control approach can improve fuel economy by 52.7% and 37.7% in Case 1 and Case 2 compared to the ADVISOR approach, respectively. Since the slopes in Case 2 are not longer and steeper than those in Case 1 the fuel economy improvement is less significant. The driving situation in Case 2 is not worse than that in Case 1, the ADVISOR approach can get better fuel economy. Since the fuel economy is calculated by the high fidelity map of the real engine, which is the most accurate evaluating method in

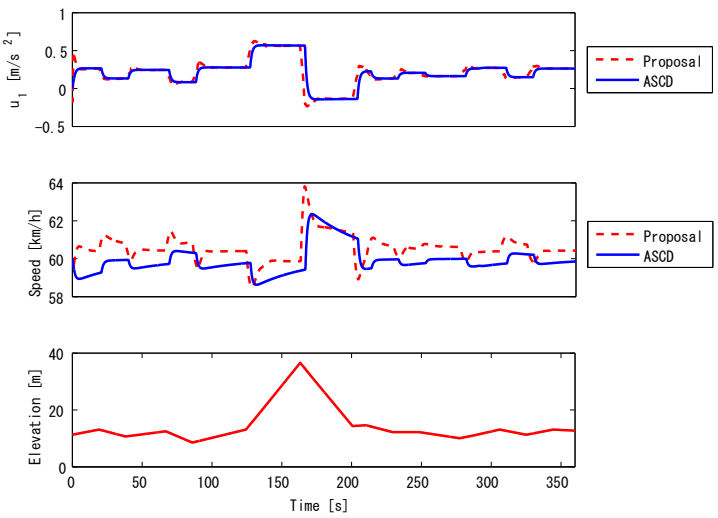

Figure 3.3.5: Driving profile of the real-time optimal control algorithm and the ASCD algorithm in Case 2.

the computer simulation environment, these results are promising.

Table 3.3.1: Fuel economy comparison results for the unknown driving pattern with slope information

Method	Case	Initial SOC	Final SOC	Fuel economy [km/l]
Proposal	Case 1	0.700	0.712	27.8(+52.7%)
ADVISOR	Case 1	0.700	0.676	18.2
Proposal	Case 2	0.700	0.695	29.2(+37.7%)
ADVISOR	Case 2	0.700	0.677	21.2

The proposed algorithm is fast for computation. The computer simulation time for the two cases is 360 [s]. The computation time of the proposed algorithm for Case 1 is 23.33 [s]. The computation time of the proposed algorithm for Case 2 is 28.10 [s]. The simulation is run in a Matlab/Simulink environment using a laptop with an Intel processor at 2.27 [GHz] processing speed and 2 [GB] of RAM. The sampling interval for the two cases is 100 [ms]. The

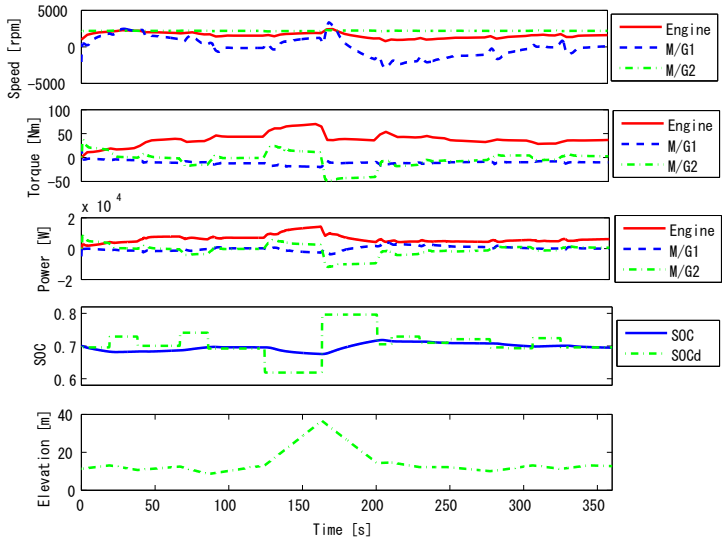

Figure 3.3.6: Power-split profile of the vehicle using the real-time optimal control algorithm in Case 2.

computation time per sampling interval of the proposed algorithm for Case 1 is 6.48 [ms]. The computation time per sampling interval of the proposed algorithm for Case 2 is 7.81 [ms]. So we can conclude that the proposed algorithm has the potential for real-time vehicle control.

3.4 Simulation results for the unknown driving pattern with slope and traffic information

3.4.1 Comparison controllers

There are five simulations in this work. They are the vehicle tracking nonlinear real-time optimal control (TROC) approach which is the proposed method, the vehicle tracking ADVISOR (TADVISOR) approach, the solitude real-time optimal control (SROC) approach,

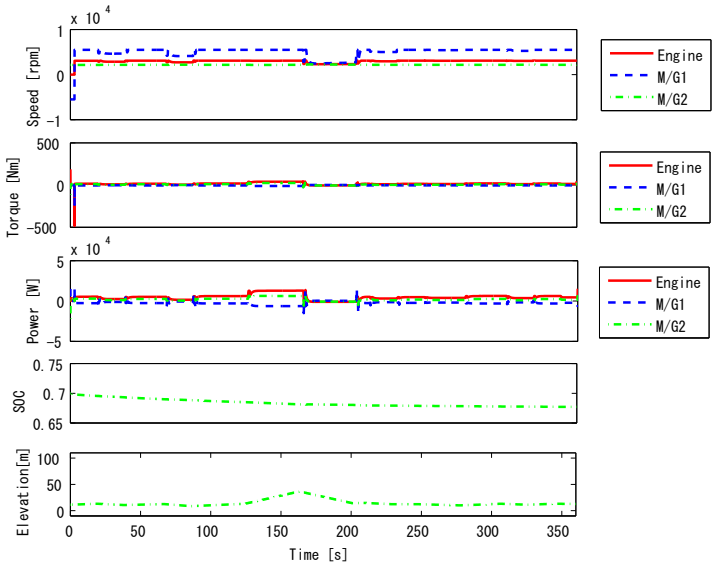

Figure 3.3.7: Power-split profile of the vehicle using the ADVISOR rule-based algorithm in Case 2.

the solitude ADVISOR (SADVISOR) approach, and the fixed battery SOC_d vehicle tracking real-time optimal control (FTROC) approach. The rule-based control for HEVs introduces a set of rules to decide the power split between the engine and the battery after the vehicle states are observed. We used the ADVISOR rule-based control approach as a comparison for the proposed vehicle tracking nonlinear real-time optimal control approach. The driving pattern used in vehicle tracking ADVISOR approach is obtained from an adaptive cruise control (ACC) method [85]. The control input of the tracking vehicle using the ACC method is calculated as follows [85]:

$$u_{ACC}(t) = \frac{v_p(t) - v(t) - k\big(hv(t) + d_{min} - (p_p(t) - p(t) - l_p\big)}{h} \tag{3.4.1}$$

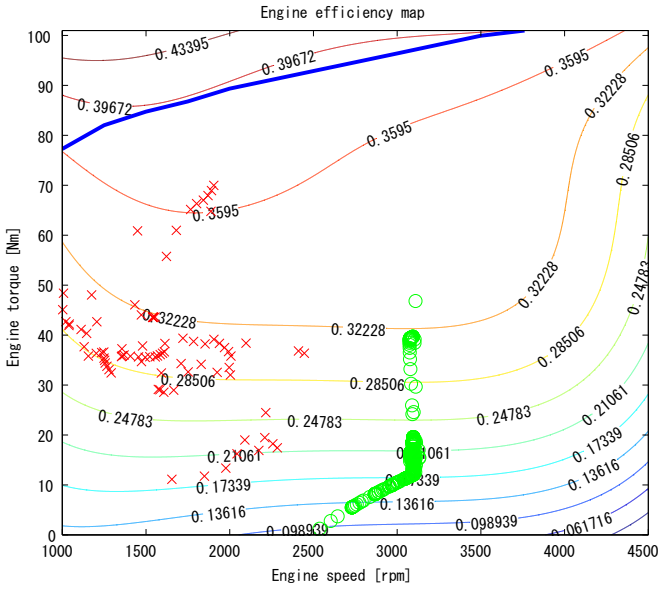

Figure 3.3.8: Engine operating point distribution using the real-time optimal control algorithm and the ADVISOR rule-based algorithm in Case 2.

where k and h are constant parameters set as $k = 0.08$ and $h = 0.15$, respectively. The preceding vehicle is controlled using the same algorithm as that in this chapter without the vehicle spacing cost term. This method is denoted as a solitude real-time optimal control method. It is a kind of eco-driving method using the real-time optimal control approach. The driving pattern used in the solitude ADVISOR approach is obtained from the automatic speed control device (ASCD). ASCD is a kind of proportional-integral control method without slope previews.

3.4.2 Test road slope profiles and calculation of the road slopes and the desired battery state of charge

The effectiveness of the proposed energy management system of the power-split HEV is evaluated using the slope information of a real road. It is a road from the Imajuku traffic light position to the Hatae traffic light position which is 6.2 [km] located at Route 202, Fukuoka, Japan. The maximum slope of this road is 3.65%, and the minimum slope of this road is -3.46%. This real terrain is typical in Japan where there are many hilly areas.

The slope information is approximated by the sigmoid functions as follows:

$$\theta(p) = \frac{s_1}{1 + e^{(s_3(p-s_2))}} + \frac{s_4}{1 + e^{(s_6(p-s_5))}} + \cdots \tag{3.4.2}$$

where $s1$, $s2$, $s3$, $s4$, $s5$, and $s6$ are slope shape parameters.

The desired battery SOC is assumed using the function as

$$\begin{aligned} &SOC_d(p) = \\ &k_{SOC}(\frac{s_1}{1 + e^{(s_3(p-s_2))}} + \frac{s_4}{1 + e^{(s_6(p-s_5))}} + \cdots) + SOC_k. \end{aligned} \tag{3.4.3}$$

where k_{SOC} and SOC_k are constant parameters set as $k_{SOC} = -2.5$ and $SOC_k = 0.71$, respectively.

3.4.3 Simulation conditions

In this simulation, vehicle parameters are used from ADVISOR 2002 [91]. The vehicle parameters are m=1504 [kg], ρ=1.23 [kg/m^3], C_D=0.3, A=1.746 [m^2], g=9.8 [m/s^2], μ=0.015, V_{OC}=307.85 [V], R_{batt}=1.004 [Ω], Q_{batt}=6 [Ah], r_w=0.287 [m], g_f=3.93, I_{eng}=0.18 [kgm^2], $I_{M/G1}$=0.0226 [kgm^2], $I_{M/G2}$=0.0226 [kgm^2], I_w=3.3807 [kgm^2], a=40.88, b=1576, c=$-$0.004051, h=1032000, k=365.7, l=$-$2.401, S=30, R=78, and l_p=4.31 [m]. The control parameters are T=10 [s], the sampling period h=0.1 [s], SOC_d=0.7, SOC_{min}=0.6, SOC_{max}=0.8, $\tau_{M/G2max}$=305 [Nm], $\tau_{M/G2min}$=$-$305 [Nm], $\tau_{M/G1max}$=55 [Nm], $\tau_{M/G1min}$=$-$55 [Nm], $\tau_{brakemax}$=2655 [Nm], $P_{battmin}$=$-$23.684 [kW], $P_{battmax}$=23.684 [kW], v_d=60 [km/h], ω_{engmax}=418.8790 [rad/s], $\omega_{M/G2max}$=628.3185 [rad/s], $\omega_{M/G1min}$=$-$575.9587 [rad/s], $\omega_{M/G1max}$=575.9587 [rad/s], d_{min}=1 [m], w_x=27000, w_y=9000, w_z=800, w_d=50000000, w_e=260000, w_f=10000, w_g=50000, w_h=10, w_i=0.1, w_j=0.1, w_k=1000, and w_l=90. The nonlinear real-time optimal control problem is solved using the numerical computation method: the continuation and generalized minimum residual (C/GMRES) method [96]. The C/GMRES method uses forward difference approach, and discretizes the HEV plant with a sampling interval h to implement the nonlinear real-time optimal control algorithm. The flowchart of the nonlinear real-time optimal control algorithm implementation is shown in Fig. 3.4.1. The nonlinear real-time optimal control control algorithm is realized by utilizing the C MEX S-function builder in Matlab/Simulink. Direct control input torque of the engine, the two M/Gs, and the mechanical brake are given by the nonlinear real-time optimal controller. The fuel economy is calculated using the engine fuel consumption map which is obtained from ADVISOR 2002.

3.4.4 Simulation results

The first column of Fig. 3.4.2 is the road elevation. The next seven columns show the vehicle control input, the optimized vehicle speed, and the vehicle spacing. The vehicle tracking nonlinear real-time optimal control vehicle predicts the upcoming up-down hills, and avoids the abrupt acceleration or deceleration as shown in the ACC method at the link parts of different slopes. The vehicle tracking nonlinear real-time optimal control algorithm gets almost the same driving profile as the solitude real-time optimal control algorithm, which validates the effectiveness of the car following model. The vehicle spacing is kept above the minimum using both methods. Instead of converging to a value, the vehicle tracking nonlinear real-time optimal control approach can make good use of the vehicle spacing range to get better fuel economy with the predicted preceding eco-driving vehicle information. In this way the vehicle tracking nonlinear real-time optimal control algorithm helps to improve the fuel economy.

Fig. 3.4.3 shows the power-split profile of the solitude real-time optimal control algorithm. The columns of Fig. 3.4.3 from the top are the road elevation, the battery SOC, the speed of the engine and the two M/Gs, the torque of the engine and the two M/Gs, and the power of the engine and the two M/Gs. Fig. 3.4.4 shows the power-split profile of the fixed battery SOC_d vehicle tracking real-time optimal control algorithm. The fixed battery SOC_d is 0.7. Fig. 3.4.5 shows the power-split profile of the vehicle tracking nonlinear real-time optimal control algorithm. There is some causality between the road elevation and the battery SOC. The lowest point of the road elevation corresponds to the highest point of the battery SOC. The highest point of the road elevation corresponds to the lowest point of the battery SOC. By using the slope information in advance to better use the battery SOC range, the vehicle

tracking nonlinear real-time optimal control algorithm helps to reduce the fuel consumption efficiently.

Overall, the solitude real-time optimal control approach uses the M/Gs to drive the vehicle compared with the vehicle tracking real-time optimal control approach, which helps to improve the fuel economy. The vehicle tracking real-time optimal control approach uses the engine fuel energy to drive the vehicle instead of the free energy recovered by the battery, which results in worse fuel economy. The solitude real-time optimal control algorithm can charge or discharge the battery more freely without the vehicle spacing constraint, so it does not use the engine to drive the vehicle during the cruising low road load period when the battery SOC is high. The power-split profile of the fixed battery SOC_d vehicle tracking real-time optimal control algorithm is roughly the same as the power-split profile of the vehicle tracking nonlinear real-time optimal control algorithm with varied battery SOC_d. Since the slopes in this real case are short and gentle, the fuel economy improvement is not significant using the vehicle tracking nonlinear real-time optimal control algorithm with varied battery SOC_d compared with the fixed battery SOC_d vehicle tracking real-time optimal control algorithm. Fig. 3.4.6 shows the power-split profile of the vehicle tracking ADVISOR algorithm. We can see that without slope previews, the engine and the M/Gs work abruptly, especially at the beginning of the simulation; and the link parts of different slopes. The battery SOC decreases continually. The vehicle does not get the regenerative braking energy properly.

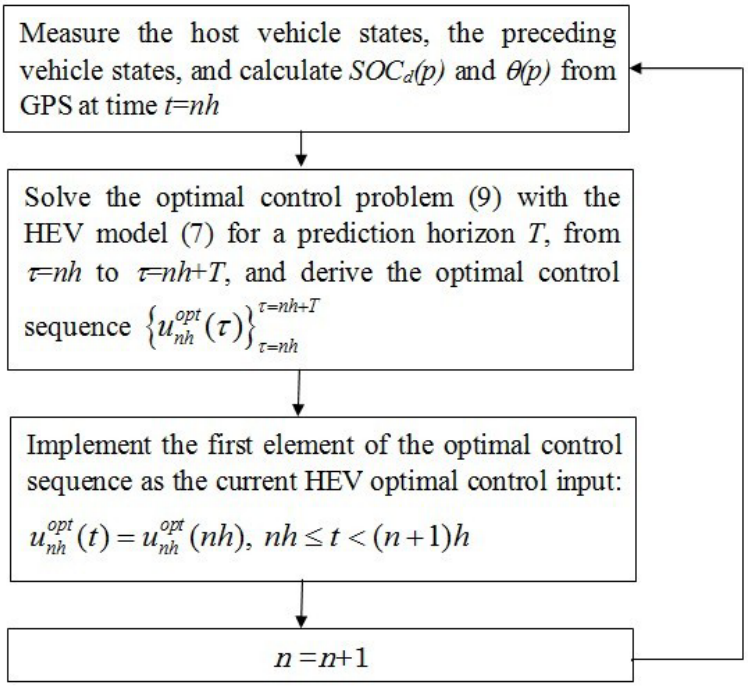

Figure 3.4.1: Flowchart of the nonlinear real-time optimal control algorithm.

A significant benefit of the power-split architecture is the fact that it decouples the engine crankshaft from the road, and allows the electric machines to move the engine speed where fuel efficiency is maximized [97]. This is identified by the engine operating point distribution in Fig. 3.4.7 and Fig. 3.4.8. Fig. 3.4.7 shows the distribution of the engine operating points of the solitude real-time optimal control algorithm and the solitude ADVISOR algorithm. Fig. 3.4.8 shows the distribution of the engine operating points of the vehicle tracking nonlinear real-time optimal control algorithm and the vehicle tracking ADVISOR algorithm. The line at the top left corner is the engine max torque line. The engine operating points cannot go beyond the line. Fig. 3.4.9 shows the distribution of the engine operating points of the fixed battery SOC_d vehicle tracking real-time optimal control algorithm.

As shown in Fig. 3.4.7 and Fig. 3.4.8 the nonlinear real-time optimal control approach

operates the engine at fairly low speed and high torque, which means high engine efficiency and low brake specific fuel consumption values. The nonlinear real-time optimal control approach forces the engine to work regularly near the engine low fuel consumption rate areas. In contrast, the ADVISOR rule-based approach operates the engine at fairly high speed and low torque, which means low engine efficiency and high brake specific fuel consumption values. By adapting the battery power to the future road load, the nonlinear real-time optimal control approach develops the ability of the power-split architecture. We can see that the engine operating points of the real-time optimal control algorithm are distributed in better areas than those of the ADVISOR algorithm. Compared with the vehicle tracking real-time optimal control approach, the solitude real-time optimal control engine operating points are distributed closer to the left corner of the engine fuel consumption map that consumes less fuel. The nonlinear real-time optimal control algorithm can make the engine work in better areas rather than those along the best efficiency line of the engine using the CVT. The fuel efficiency depends on the real efficiency of the engine, which makes the point that a high efficiency area is more profitable. The engine operating point distribution of the fixed battery SOC_d vehicle tracking real-time optimal control algorithm is roughly the same as the engine operating point distribution of the vehicle tracking nonlinear real-time optimal control algorithm with varied battery SOC_d. This confirms that the fuel model utilized in this work is accurate, and the vehicle tracking nonlinear real-time optimal control algorithm is effective to find the global optimal values.

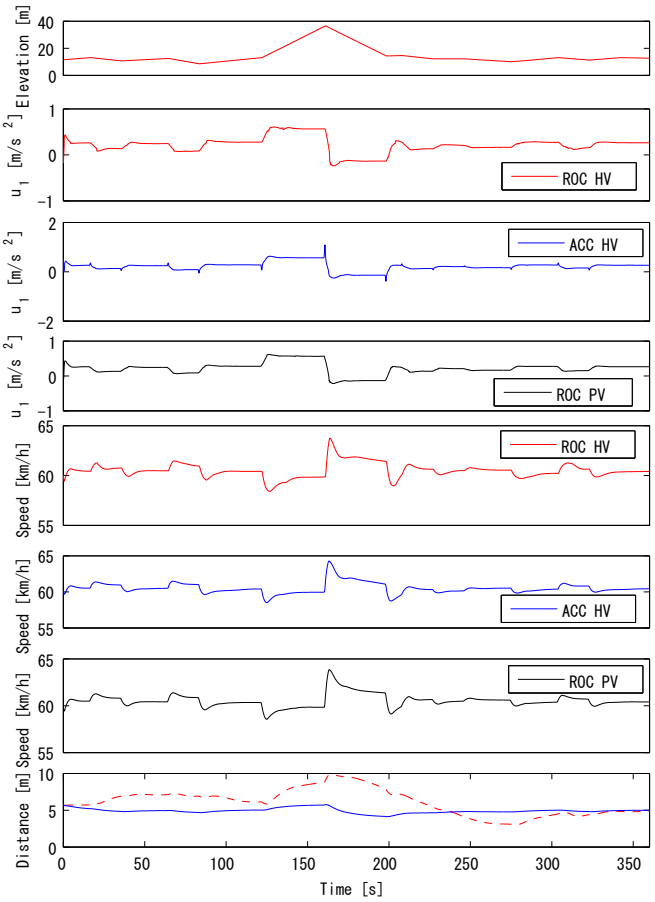

Figure 3.4.2: Driving profile of the vehicle tracking nonlinear real-time optimal control algorithm and the ACC algorithm. PV represents the preceding vehicle, HV represents the host vehicle.

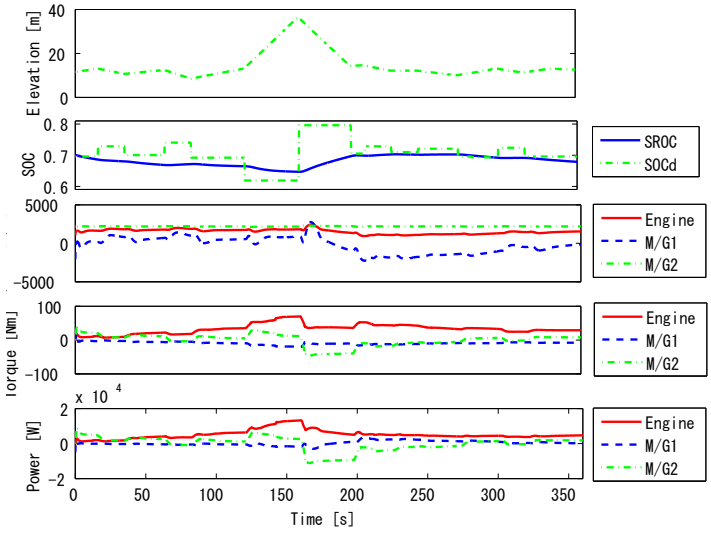

Figure 3.4.3: Power-split profile of the vehicle using the solitude real-time optimal control algorithm.

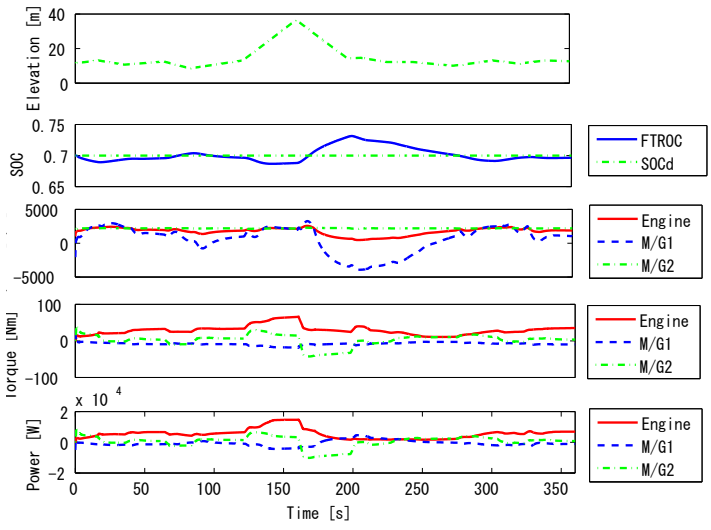

Figure 3.4.4: Power-split profile of the vehicle using the fixed desired battery SOC vehicle tracking real-time optimal control algorithm.

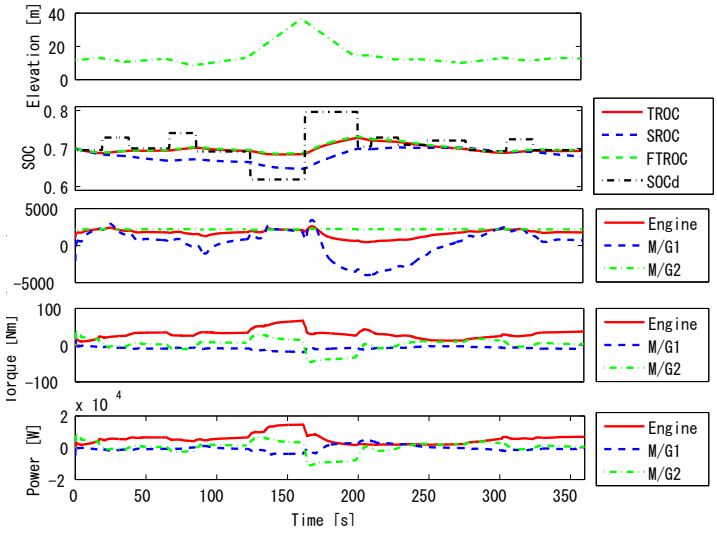

Figure 3.4.5: Power-split profile of the vehicle using the vehicle tracking nonlinear real-time optimal control algorithm.

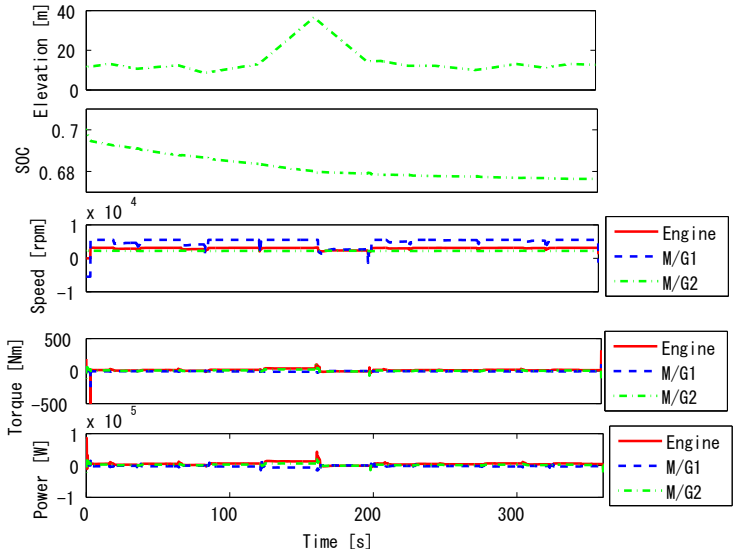

Figure 3.4.6: Power-split profile of the vehicle using the vehicle tracking ADVISOR rule-based algorithm.

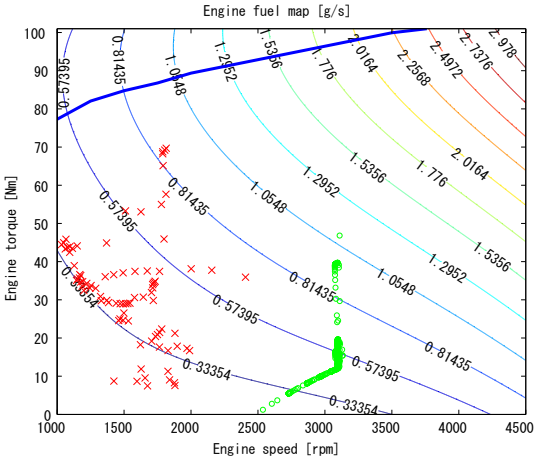

Figure 3.4.7: Engine operating point distribution using the solitude real-time optimal control algorithm and the solitude ADVISOR rule-based algorithm. The crosses and the circles denote the engine operating points of the solitude real-time optimal control algorithm and the solitude ADVISOR algorithm, respectively.

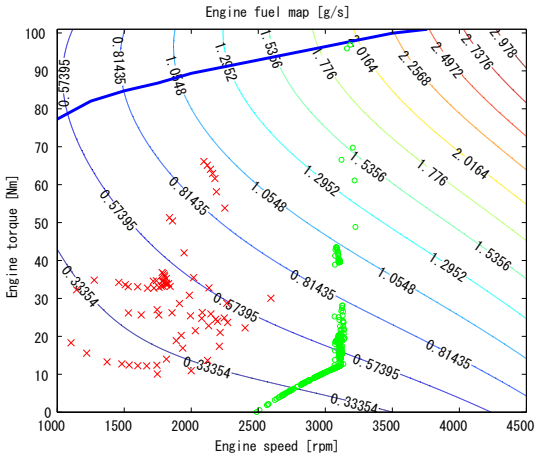

Figure 3.4.8: Engine operating point distribution using the vehicle tracking nonlinear real-time optimal control algorithm and the car tracking ADVISOR rule-based algorithm. The crosses and the circles denote the engine operating points of the vehicle tracking nonlinear real-time optimal control algorithm and the vehicle tracking ADVISOR algorithm, respectively.

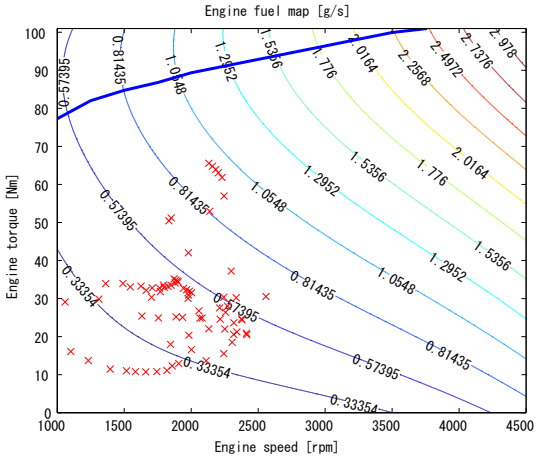

Figure 3.4.9: Engine operating point distribution using the fixed desired battery SOC vehicle tracking real-time optimal control algorithm.

The overall fuel economy results are presented in Table 3.4.1. We can see that the vehicle tracking nonlinear real-time optimal control approach can improve fuel economy by 47.24% compared to the solitude ADVISOR approach. Since the vehicle tracking ADVISOR approach cannot avoid the acceleration or deceleration spikes at the link parts of different slopes, it gets worse fuel economy than that using the solitude ADVISOR approach. We can see from Fig. 3.4.5 and Table 3.4.1 that better using of the battery SOC range results in better fuel economy. This leads to better fuel economy using the solitude real-time optimal control approach than the vehicle tracking real-time optimal control approach. By using the predicted road slope information freely, the solitude real-time optimal control algorithm can adapt the HEV battery SOC profile according to the known bounds of the parameters to get better fuel economy. Although the slopes in this real case are short and gentle, the vehicle tracking nonlinear real-time optimal algorithm with varied battery SOC_d achieves better fuel economy compared with the fixed battery SOC_d vehicle tracking real-time optimal control algorithm. The varied battery SOC_d approach utilizes the future road load information,

and can obtain desired actuator operation compared to the fixed battery SOC_d approach. Since the fuel economy is calculated by the high fidelity map of the real engine, which is the most accurate evaluating method in the computer simulation environment, these results are promising.

Table 3.4.1: Fuel economy comparison results for the unknown driving pattern with slope and traffic information

Method	Initial SOC	Final SOC	Fuel economy [km/l]
Tracking ROC	0.7000	0.6938	31.23(+47.24%)
Tracking ADVISOR	0.7000	0.6768	21.00(-0.99%)
Fixed tracking ROC	0.7000	0.6965	30.66(+44.55%)
Solitude ROC	0.7000	0.6988	34.47(+62.52%)
Solitude ADVISOR	0.7000	0.6772	21.21(+0.00%)

The proposed vehicle tracking nonlinear real-time optimal control algorithm is fast for computation. The computer simulation time is 360 [s]. The computation time of the proposed vehicle tracking nonlinear real-time optimal control algorithm is 23.10 [s]. The simulation is run in a Matlab/Simulink environment using a laptop with an Intel processor at 2.27 [GHz] processing speed and 2 [GB] of RAM. The sampling interval is 100 [ms]. The computation time per sampling interval of the proposed vehicle tracking nonlinear real-time optimal control algorithm is 6.42 [ms]. So it is concluded that the vehicle tracking nonlinear real-time optimal algorithm has the potential for real-time vehicle control.

3.5 Discussion for the simulation for unknown driving patterns

For real-time implementation, the fuel model needs to be continuous and differentiable. The fuel model needs simplifications and also to be accurate enough. It is different from the engine map model which cannot be predictable and implemented in real-time. As for the physical constraint, it is guaranteed by the second term of the cost function. The discontinuous jump of the engine speed will cause the discontinuous fly of the vehicle speed because of the planetary set. This will lead a very large punitive value of the vehicle acceleration which is included in the second term of the cost function.

CHAPTER IV

Optimal energy management of plug-in hybrid electric vehicles with uncertain driving distance

This chapter presents the modeling, control, and simulation of plug-in hybrid electric vehicles with uncertain driving distance. This chapter is organized as follows. Section 2.1 introduces the features of the approach. Section 2.2 presents the modeling and control for the 1 degree of freedom model. Section 2.3 provides the simulation results with uncertain driving distance. Section 2.4 presents the discussion.

4.1 Features of the approach with uncertain driving distance

The proposed method is extended when the driving distance is unknown. The fuel economy improvements for the PHEV are confirmed with driving distance uncertainty in reality using the proposed nonlinear real-time optimal control method. The proposed controller can

be constructed without the trip distance information which is required in the conventional control method.

4.2 modeling and control for the 1 degree of freedom model

The 1 degree of freedom model in Chapter II is also utilized in this PHEV system.

The optimal controller is also divided into two levels. The high-level controller finds the optimal battery power, and the low-level controller determines the optimal torque and speed of the engine and the motor/generators.

This work proposes two control strategies: the charge depletion strategy and the all-electric charge depletion followed by charge sustenance control strategy. There are two PHEV operating modes to be optimized in the two proposed control strategies. They are charge depleting (CD) mode and charge sustaining (CS) mode. The optimal control problem corresponding to the charge sustaining mode is formulated as

$$\text{Minimize: } J = \frac{1}{2}(x_{SOC} - x_f(t+T))^T S_f(x_{SOC} - x_f(t+T))$$
$$+ \int_t^{t+T} L_{CS}(x_{SOC}(\tau|t), P_{batt}(\tau|t))d\tau \tag{4.2.1}$$
$$\text{Subject to: } P_{battmin} \leq P_{batt}(\tau|t) \leq P_{battmax} \tag{4.2.2}$$

where T is the prediction horizon; x_f is the desired final state value; S_f is the weight; and $P_{battmin}$ and $P_{battmax}$ denote the minimum battery power and the maximum battery power.

The objective of this optimal control problem is to minimize the fuel consumption, while

the battery SOC is maintained between the thresholds. This is achieved by minimizing the cost function L_{CS}, which includes four terms: the fuel consumption, the engine use and the mechanical brake use, the deviation of battery SOC from the reference value, and the penalization of state constraint violations. The cost function L_{CS} is defined as follows:

$$\begin{aligned} L_{CS} &= w_1 c_f (P_{req} - P_{batt})/(1 + e^{-\beta(P_{req}-P_{batt})}) \\ &+ w_2 (P_{req} - P_{batt})^2 + w_3 \left(\frac{1}{2}(x_{SOC} - SOC_d)\right)^2 \\ &+ w_4(-\ln(x_{SOC} - SOC_{minlow}) - \ln(SOC_{maxup} - x_{SOC})) \end{aligned} \tag{4.2.3}$$

where SOC_d is the desired battery SOC value; w_1, w_2, w_3 and w_4 are the weights; SOC_{minlow} and SOC_{maxup} denote the minimum battery SOC and the maximum battery SOC during the charge sustaining mode. The log barrier function is introduced as a penalizing term for violations of state constraints which are hard to be dealt with. The performance index value becomes very large when the state constraint is being violated. By doing so, the state constraint of the nonlinear system is satisfied automatically.

The two $P_{req}-P_{batt}$ terms have different roles. The first $P_{req}-P_{batt}$ term is for fuel economy evaluation using the Willan's line method. The sigmoid function in the term will lead the fuel consumption to 0 when the vehicle slows down. The quadratic penalty $P_{req} - P_{batt}$ term is introduced to make best use of the battery energy buffer and avoid using engine power. This term can predict the future road load to adapt the battery power to the future road load.

The optimal control problem corresponding to the charge depleting mode is formulated

as

$$\text{Minimize: } J = \int_t^{t+T} L_{CD}(x_{SOC}(\tau|t), P_{batt}(\tau|t))d\tau \tag{4.2.4}$$

$$\text{Subject to: } P_{battmin} \leq P_{batt}(\tau|t) \leq P_{battmax} \tag{4.2.5}$$

The objective of this optimal control problem is to minimize the fuel consumption, while the battery charge is depleted to the minimum. This is achieved by minimizing the cost function L_{CD}, which includes four terms: the fuel consumption, the penalization of state constraint violations, the engine use and the mechanical brake use, and the battery power use. The cost function L_{CD} is defined as follows:

$$\begin{aligned} L_{CD} &= w_x c_f (P_{req} - P_{batt})/(1 + e^{-\beta(P_{req} - P_{batt})}) \\ &+ w_d(-\ln(x_{SOC} - SOC_{minlow}) - \ln(SOC_{max} - x_{SOC})) \\ &+ w_y(P_{req} - P_{batt})^2 + w_e P_{batt} \end{aligned} \tag{4.2.6}$$

where w_x, w_y, w_d, and w_e are the weights; SOC_{max} is the maximum battery SOC during the charge depleting mode. The last term concerning the battery power use is inspired by the equivalent consumption minimization strategy (see [62]– [71]). The equivalent consumption minimization strategy assumes that the current battery energy use will cost the same amount of fuel energy in the future as it does in the current driving conditions [7]. So this term can control the speed of battery charge depleting.

Since the future road load is known in advance, the authors believe that it is natural and simple to adapt the battery power to the future road load to obtain better fuel economy. This relationship is clearly formulized as the term of the cost function to reduce the use of

the engine or the mechanical brakes in the optimal control problem. It can make best use of the battery energy buffer. The battery can assist the vehicle driving during the acceleration process, and recuperate the free brake energy during the deceleration process. The engine operating points can also be shift to the engine optimal operating line by this adaption.

The inequality constraint in the optimal control problems is converted to an equality constraint by introducing a dummy input u_d for computation simplicity as follows:

$$C(x(t), u(t)) = u^2(t) + u_d^2(t) - P_{battmax}^2 = 0 \tag{4.2.7}$$

where $P_{battmax}$ has the same absolute value but the opposite sign as $P_{battmin}$.

To solve these optimal control problems with the calculus of variation method [94], the Hamiltonian function is defined by

$$H(x, u, \lambda, \psi) = L(x, u) + \lambda^T f(x, u) + \psi^T C(x, u) \tag{4.2.8}$$

where λ denotes the co-state, and ψ denotes the Lagrange multiplier associated with the equality constraint.

The first-order necessary conditions for the optimal control input u, the multiplier ψ, and the co-state λ are obtained using the calculus of variation as

$$\begin{aligned}
&\dot{x} = f(x, u) \quad x(t_0) = x_0 \\
&\dot{\lambda} = -\left(\frac{\partial H}{\partial x}\right)^T \quad \lambda_{CD}(t+T) = 0 \quad \text{or} \quad \lambda_{CS}(t+T) = S_f(x_{SOC} - x_f(t+T)) \\
&\frac{\partial H}{\partial u} = 0 \\
&C(x, u) = 0
\end{aligned} \tag{4.2.9}$$

where t_0 is the initial time, and x_0 is the initial state.

The derivative of the co-state λ concerning the battery SOC is obtained as

$$\begin{aligned}\dot{\lambda} &= -w_3(x_{SOC} - SOC_d) \\ &-w_4\left(\frac{1}{SOC_{max} - x_{SOC}} - \frac{1}{x_{SOC} - SOC_{min}}\right).\end{aligned} \tag{4.2.10}$$

The battery SOC co-state is affected by the battery desired SOC and the bounds of the battery SOC. A large co-state will lead to the small variation of the battery SOC. And a small co-state will lead to the large variation of the battery SOC. Well tuned performance indices and weights can lead to a better system.

4.3 Simulation results with uncertain driving distance

4.3.1 Comparison controllers

There are four simulations in this work. They are the all-electric charge depletion followed by charge sustenance control (CDCS) approach using the proposed real-time optimal control, the charge depletion control (CD) approach using the proposed real-time optimal control, CDCS using the stochastic dynamic programming control (SDP) approach [8], and CD using the SDP approach [8]. The first two approaches are the proposed methods in this paper. The driving distance of the 2 FTP-72 cycles simulated back-to-back for the four simulations is 24.14 [km]. The battery capacity for the proposed two approaches is 2.62 [kWh]. The battery capacity for the two SDP approaches is 3.46 [kWh]. The stochastic dynamic programming control approach proposed by the authors of [8] utilized the 2002 Toyota HEV Prius model

with a double battery capacity. The two proposed real-time optimal control approaches used the 2004 Toyota HEV Prius model with a double battery capacity. PHEV parameters are not publicized in detail. The battery capacity of the Toyota Prius PHEV is about three times as that of the Toyota Prius HEV. The battery capacity tends to be enlarged in PHEVs. If possible, the author wants to use the Toyota Prius PHEV parameters; however, the author had to use the parameter of the known Toyota Prius HEV. The battery capacity which is 3 times as that of the original 2004 Toyota Prius HEV is not used to avoid too much difference from the original HEV and unreality e.g. overweight or over voltage. The battery parameters in this work are battery capacity of 2.62 [kWh], system voltage of 403.0 [V], battery resistance of 0.638 [Ω]. The battery parameters in the SDP approach are battery capacity of 3.46 [kWh], system voltage of 615.8 [V], battery resistance of 2.000 [Ω]. The power loss of the battery is directly proportional to the square of the voltage and is inversely proportional to the resistance. The fuel economy advantages of the propose system is at best 25% compared with that using the model in the SDP approach only considering the battery effect. The fuel improvement using the proposed approach is 58%. The effectiveness of the proposed approach is still preferable compared with the SDP approach. Since the model of the two SDP approaches is similar as that in this work, the results are comparable.

4.3.2 Simulation conditions

Effectiveness of the above proposed approach is validated by the benchmark simulator, which was provided by the Technical Committee on Automotive Control and Model Research (JSAE and SICE Joint) in SIMULINK® and GT-SUITE® [89]. The GT-SUITE engine model which contains the cam valve, thermo, intake air, throttle valve, exhaust gas dynamics has high fidelity. In this simulation, vehicle parameters are obtained from the

benchmark simulator. The only difference from the original benchmark simulator data is that the battery capacity is doubled. Specifically, the author double the original 28 modules of Ni-MH batteries in the benchmark simulator for 56 modules of Ni-MH batteries in the experimental PHEV of this work.

The total simulation time is 2738 [s] of the 2 FTP-72 cycles simulated back-to-back. The sampling time is 0.02 [s], and the prediction horizon T is 10 [s]. The vehicle parameters are m=1460 [kg], ρ=1.23 [kg/m^3], C_D=0.33, A=1.746 [m^2], g=9.8 [m/s^2], μ=0.015, V_{OC}=403.2 [V], R_{batt}=0.6384 [Ω] and Q_{batt}=6.5 [Ah], c_f=0.076. The control parameters are β=0.5, SOC_d=0.3, SOC_{minlow}=0.2, SOC_{maxup}=0.4, SOC_{max}=0.95, $P_{battmin}$=$-$30 [kW], $P_{battmax}$=30 [kW], x_f=0.3, S_f=5×10^{11}, the weights for the charge depletion strategy w_{x1}=6, w_{y1}=300, w_{d1}=0.001, and w_{e1}=2500, and the weights for the all-electric charge depletion followed by charge sustenance control strategy w_{x1}=6, w_{y1}=300, w_{d1}=0.001, and w_{e1}=1200, w_1=92, w_2=5×10^4, w_3=3.5×10^5, and w_4=0.001.

The nonlinear real-time optimal control problem is solved using the numerical computation method: the continuation and generalized minimum residual (C/GMRES) method [96]. The nonlinear real-time optimal control algorithm is realized by utilizing the C MEX S-function builder in MATLAB/SIMULINK. First, the optimal battery power is calculated by the high-level controller. Next, this optimal value is fed into the low-level controller where the optimal torque and speed of the engine and M/Gs are determined. Finally, these actual control input signals are applied to the PHEV energy management ECU simulator. The fuel economy is calculated using the benchmark simulator which is based on the GT-SUITE high fidelity vehicle model.

4.3.3 Simulation results

Fig. 4.3.1 shows the simulation results of the SDP approach. Fig. 4.3.2 shows the simulation results of the nonlinear real-time optimal control CD approach. The columns of Fig. 4.3.2 from the top are the required vehicle speed by the driving cycle, the power of M/G1, the power of M/G2, the power of the engine, and the battery SOC. The battery is depleted to its minimum allowable charge by the end of the trip. Fig. 4.3.3 shows the simulation results of the nonlinear real-time optimal control CDCS approach. At first, the vehicle is driven by M/G2 until the battery charge is depleted to its minimum at 2300 [s] of the simulation using the charge depleting mode, and then the control is switched to the charge sustaining mode. During the charge depleting mode in the above two proposed approaches, the engine can be turned on to work along its OOL if the driving power or torque requests exceed the capabilities of the battery or the motors. The battery SOC constraint is satisfied in the above two proposed simulations. The torque, speed, and power of the engine and M/Gs are reasonable according to the commercially available Toyota Prius HEV energy management ECU in the above two proposed simulations. Overall, the nonlinear real-time optimal control CD and nonlinear real-time optimal control CDCS approach use the M/Gs to drive the vehicle, which helps to improve the fuel economy. The two SDP approaches use the battery energy to drive the vehicle firstly not considering the engine optimal operating points, which results in worse fuel economy. The power-split profile of the nonlinear real-time optimal control CD algorithm is roughly the same as the power-split profile of the nonlinear real-time optimal control CDCS algorithm.

A significant benefit of the power-split architecture is the fact that it decouples the engine crankshaft from the road, and allows the electric machines to move the engine speed where

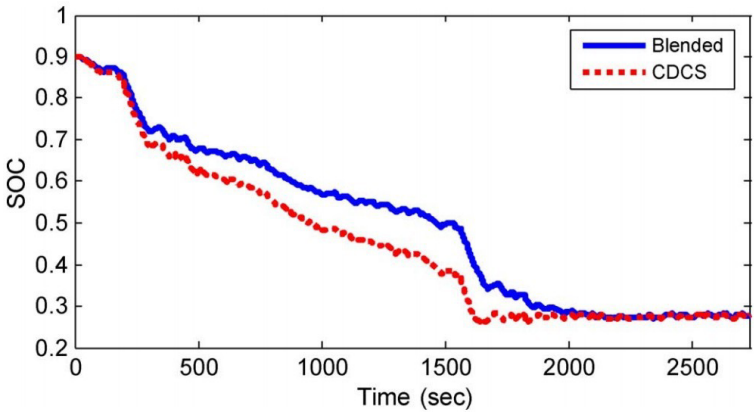

Figure 4.3.1: State-of-charge response for the blended and CDCS control strategies on two FTP-72 cycles simulated back-to-back. The blended control strategy is the same as the charge depletion control strategy is this work. Figure referred to [8]

fuel efficiency is maximized [97]. This is identified by the engine operating point distribution in Fig. 4.4.1, Fig. 4.4.2, Fig. 4.4.3, and Fig. 4.4.4. As shown in Fig. 4.4.1, Fig. 4.4.2, Fig. 4.4.3, and Fig. 4.4.4, the nonlinear real-time optimal control CD and nonlinear real-time optimal control CDCS approach operate the engine at fairly low speed and high torque, which means high engine efficiency and low brake specific fuel consumption values. The nonlinear real-time optimal control CD and nonlinear real-time optimal control CDCS approach force the engine to work regularly, above and close to the engine OOL. In contrast, the two SDP approaches operate the engine at fairly high speed and low torque, which means low engine efficiency and high brake specific fuel consumption values. By adapting the battery power to the future road load, the nonlinear real-time optimal control CD and nonlinear real-time optimal control CDCS approach develop the ability of the power-split architecture to shift the engine operating points to the engine OOL. As for the two SDP approaches, although they operate the engine at fairly low speed, the engine torque is also low, which means lower engine efficiency and higher brake specific fuel consumption values than those using

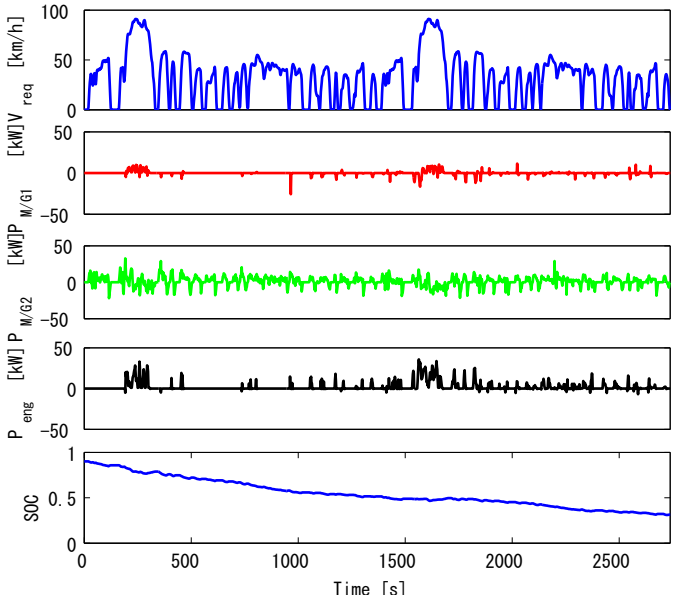

Figure 4.3.2: Simulation results of the nonlinear real-time optimal control CD approach

the nonlinear real-time optimal control CD approach and nonlinear real-time optimal control CDCS approach.

The detailed power-split characteristics of the nonlinear real-time optimal control CD approach, and the nonlinear real-time optimal control CDCS approach are shown in Fig. 4.4.5 and Fig. 4.4.6. The nonlinear real-time optimal control CD approach and the nonlinear real-time optimal control CDCS approach assist the engine when significant power is requested from the road load, recuperates the free regenerative braking energy during the deceleration period, and runs the HEV in the all-electric mode during the cruise period. All of the plug-in hybrid electric vehicle operating modes [88] and [89]: idle stop, engine charge, engine start, electric vehicle, motor assist and electric continuously variable transmission, and regenerative braking, can be realized using the proposed two nonlinear real-time optimal control approaches. All of these lead to the improvement of the fuel efficiency by making best use

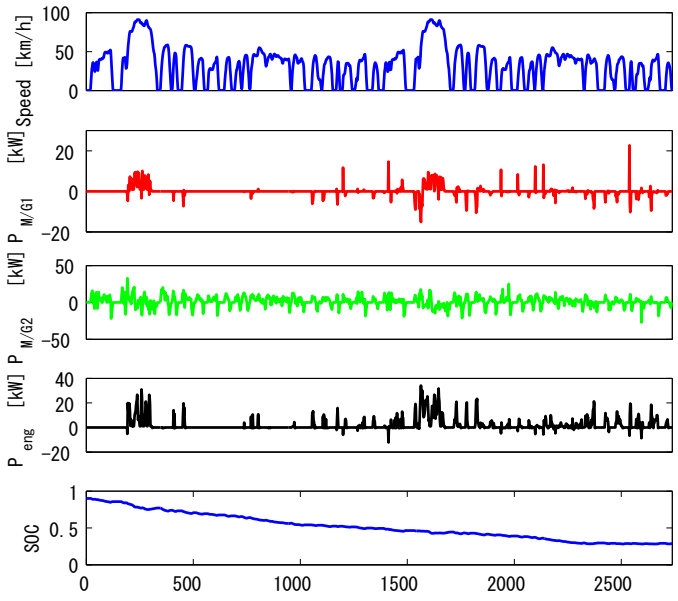

Figure 4.3.3: Simulation results of the nonlinear real-time optimal control CDCS approach

of the battery energy buffer.

Table 4.3.1 presents the overall fuel economy comparison results. We can see that the nonlinear real-time optimal control CD approach and the nonlinear real-time optimal control CDCS approach can improve fuel economy by 58.0% and 58.0% compared with the CDCS-SDP approach. The fuel economy improvements using the CD-SDP approach is less significant compared with those using the nonlinear real-time optimal control CD approach and the nonlinear real-time optimal control CDCS approach. The battery is depleted near to its minimum using the nonlinear real-time optimal control CD approach and the nonlinear real-time optimal control CDCS approach, which improves the fuel economy significantly. The nonlinear real-time optimal control CD approach and the nonlinear real-time optimal control CDCS approach get the same fuel economy but different final battery SOC. Since

Table 4.3.1: Fuel economy comparison results

Method	Initial SOC	Final SOC	Fuel economy [km/l]
CD-Proposed	0.900	0.314	44.7(+58.0%)
CDCS-Proposed	0.900	0.287	44.7(+58.0%)
CD-SDP [8]	0.900	–	30.7(+8.48%)
CDCS-SDP [8]	0.900	–	28.3

there is energy dissipated by the mechanical brake and regenerated by the battery, the phenomenon does not violate the law of conservation of energy. These results are promising because the fuel economy is calculated by the GT-SUITE high fidelity HEV model of a real engine, which is the most accurate evaluation method in the computer simulation environment.

The proposed two real-time optimal control algorithms is fast for computation. The computer simulation time is 2738 [s]. The computation time of the proposed two real-time optimal algorithms is 1800 [s]. The simulation is run in a Matlab/Simulink environment using a laptop with an Intel processor at 2.27 [GHz] processing speed and 2 [GB] of RAM. The sampling interval is 20 [ms]. The computation time per sampling interval of the proposed two real-time optimal algorithms is 13 [ms]. So it is concluded that the proposed two real-time optimal algorithms have the potential for real-time vehicle control.

4.4 Discussion

The input signals that are the road profiles are basically unknown in advance. Therefore, new modeling and control techniques are required when the trip distance is unknown. The traditional requirement of knowing the trip distance for plug-in hybrid electric vehicles is

needless by operating the engine at the best efficiency operating points of the engine using the proposed nonlinear real-time optimal control algorithm.

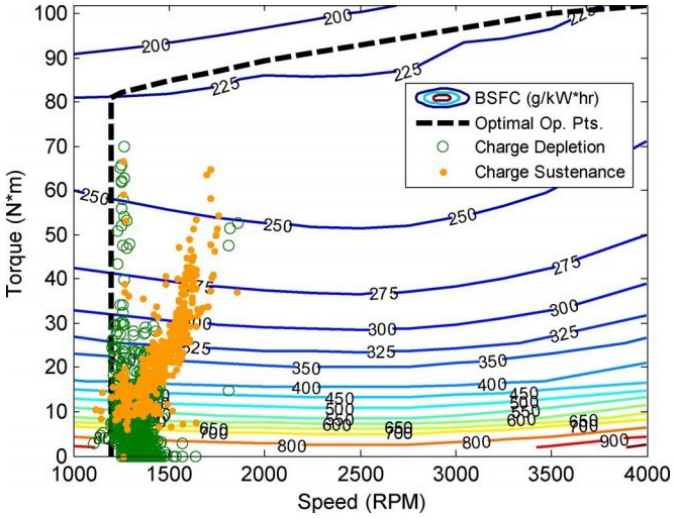

Figure 4.4.1: Engine operating points for the blended strategy on a brake specific fuel consumption map, for two FTP-72 cycles simulated back-to-back. The blended control strategy is the same as the charge depletion control strategy is this work. Figure referred to [8]

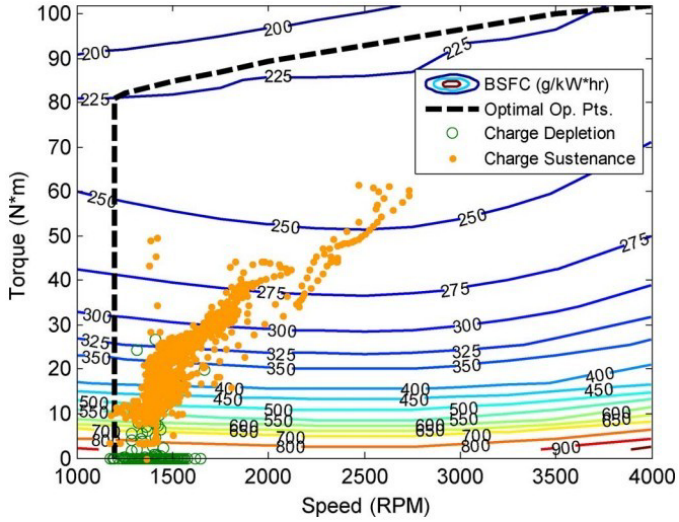

Figure 4.4.2: Engine operating points for the CDCS strategy on a brake specific fuel consumption map, for two FTP-72 cycles simulated back-to-back. Figure referred to [8]

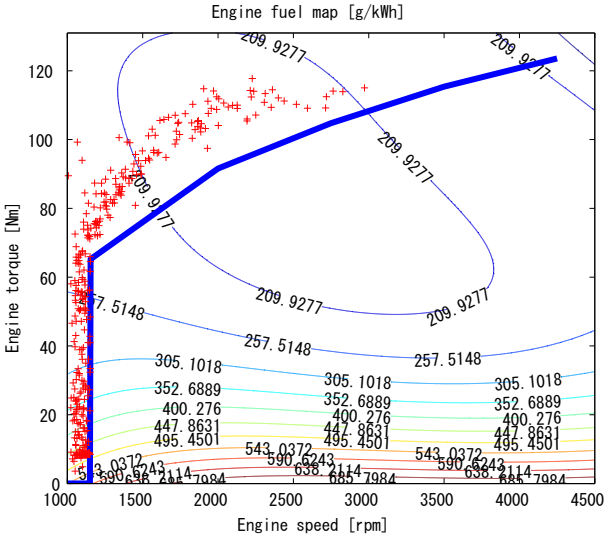

Figure 4.4.3: Engine operating point distribution using the nonlinear real-time optimal control CD approach

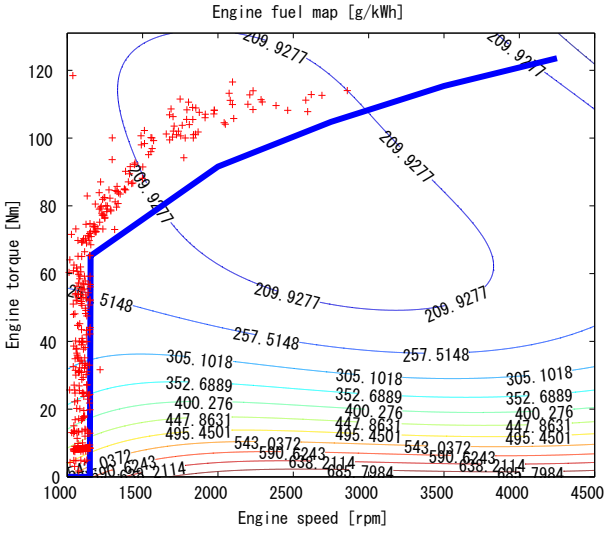

Figure 4.4.4: Engine operating point distribution using the nonlinear real-time optimal control CDCS approach

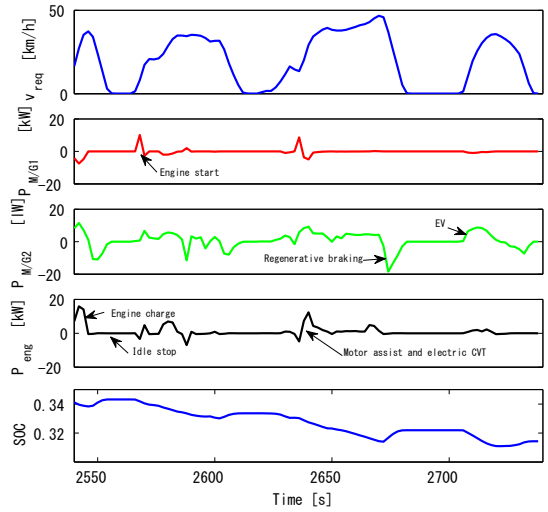

Figure 4.4.5: Detailed simulation results of the nonlinear real-time optimal control CD approach

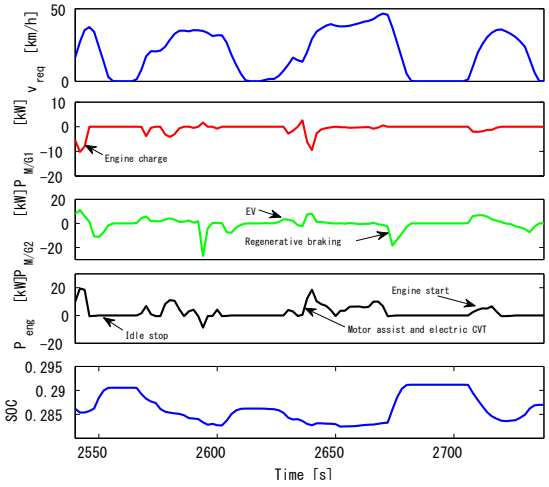

Figure 4.4.6: Detailed simulation results of the nonlinear real-time optimal control CDCS approach

CHAPTER V

Conclusions

6.1 Conclusions

In this dissertation, fuel economy real-time optimal control of HEVs and PHEVs was presented. The objective was to propose a systematic methodology for modeling, formulating, solving, and analyzing power management problems over fixed and unfixed driving cycles.

First, fuel economy improvements in the HEV are confirmed by predicting daily commuting driving cycle information using the proposed nonlinear real-time optimal control method. The apparent relationship between the battery power and the future road load is addressed in the cost function of the fuel economy optimal control problem with a simplified HEV energy management system model.

Second, fuel economy optimization of HEVs is proposed by predicting future road slopes and traffic information. The proposed method can optimize both the engine operating point and the driving profile with slope and traffic information.

Third, the proposed method is extended when the driving distance is unknown. The

fuel economy improvements for the PHEV are confirmed with driving distance uncertainty in reality using the proposed nonlinear real-time optimal control method. The proposed controller can be constructed without the trip distance information which is required in the conventional control method.

The main contribution is a systematic real-time optimal control approach for energy management in HEVs and PHEVs by predicting future road loads. This systematic design process is useful for significant fuel economy improvements in the energy management control unit application with minimal hardware cost. The conclusion is that the nonlinear real-time optimal control approach is effective for the energy management problem of the HEV/PHEV system.

6.2 Future work

There are some future directions that advance this work.

First, instead of a rule-based control algorithm, other optimal control algorithms (applied to the whole driving cycle) like dynamic programming or Pontryagin's minimum principle can be considered as comparison controllers for the proposed algorithm. The engine maximum torque constraint should be considered. The state variant constraints like the motor/generator torque and the engine speed should also be considered. Using those global optimization algorithms, the best fuel economy can be found in case of attainment of all the future driving information. The fuel economy gap between the proposed optimal control algorithm and the global optimization algorithms can be investigated.

Second, the prediction horizon length effects can be considered. Since the model in this work is complex, there is computation failure when the prediction horizon is lengthened. To

solve this problem, a sliding mode controller between the real-time optimal control algorithm and the instantaneous optimization algorithms like equivalent consumption minimization strategy may be considered.

Third, new predictive models like traffic congestion and traffic light information can be incorporated in the nonlinear real-time optimal control algorithm. The proposed real-time optimal control algorithm can be applied to energy management problems for eco-vehicles based on more realistic driving conditions instead of specified driving cycles.

Fourth, additional costs or states like emissions can be considered in the real-time optimal control algorithm. Emission reduction is another important advantage of hybrid vehicles. By adding emission constraints, better fuel economy may be obtained.

Fifth, the driver model can be incorporated in the nonlinear real-time optimal control algorithm. Since driver comfort is important recently, taking no account of the driver may hinder the application of the proposed algorithm.

APPENDICES

APPENDIX A
ENGINE FUEL CONSUMPTION MODEL

The proposed engine fuel consumption modeling method is a special method using both Willan's line method [93] and the assumption of operating the engine along the engine optimal operating line, and is introduced as follows. The HEV parameters are used from the ADVISOR 2002 Toyota Prius HEV data [81].

In [93], the Willan's line model consists of an affine representation relating the available energy, that is, the energy that is theoretically available for conversion, to the useful energy that is actually present at the output of the energy converter. Formally

$$W_{out} = eW_{in} - W_{loss} \tag{6.0.1}$$

Where the parameter e represents the peak intrinsic energy conversion efficiency of the converter, and W_{loss} represents external (parasitic) losses. In fact, this model of energy conversion efficiency is nonlinear, in that the parameters e and W_{loss} are represented as explicit functions of the output flow variable (e.g., engine speed) and are also implicit functions of the effort variable.

The modelling method given above is for general engines. However, in this work, the electric CVT can realize idle stop, so W_{loss} becomes zero. When it is assumed that the engine operating points are maintained at the best efficiency, the parameters e can be approximated

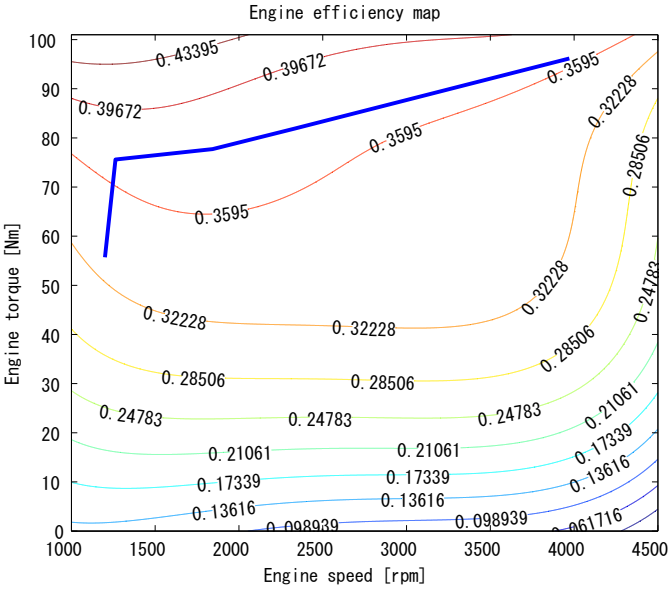

Figure 6.0.1: The engine efficiency map to the best engine operating points

as a constant. In this case, the fuel consumption rate corresponding to the optimal operating line can be fitted using a linear function.

The engine optimal operating line can be plotted on the engine map as shown in Fig. 6.0.1. The engine optimal operating points provide the highest efficiency for a given power level. The engine best efficiency related to the engine power according to the engine characteristics is shown in Fig. 6.0.2.

The fuel consumption rate is estimated as (see Fig. 6.0.3)

$$\dot{m}_f = \frac{P_{eng}}{C\eta} \approx c_f P_{eng} \tag{6.0.2}$$

where C is the calorific value of the gasoline, which is equal to 34.5×10^6 [J/l], and η is the engine efficiency.

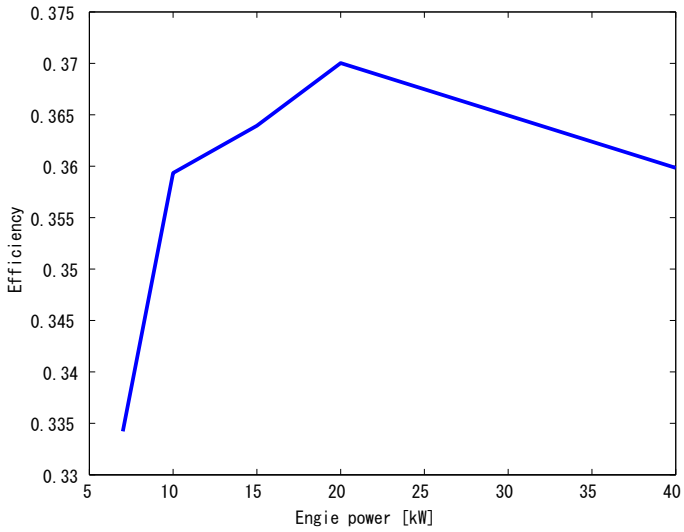

Figure 6.0.2: The engine efficiency curve to the best engine operating points

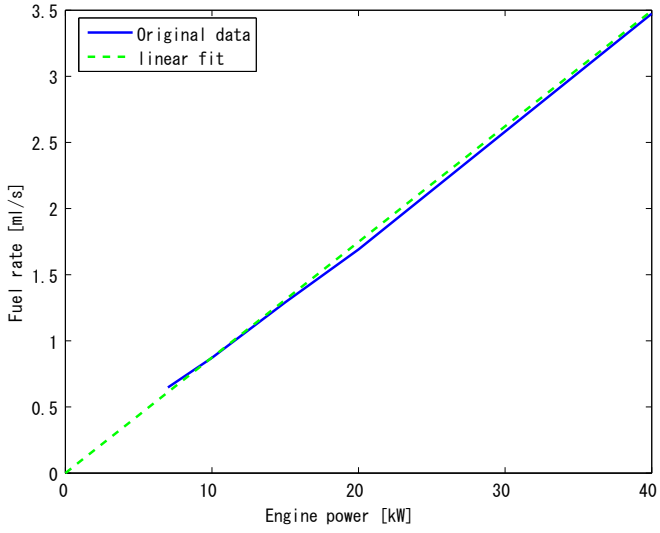

Figure 6.0.3: The engine fuel consumption rate to the best engine operating points

APPENDIX B
SOLUTION OF THE REAL-TIME OPTIMAL CONTROL PROBLEM

A brief description of the solution of the real-time optimal control problem is provided as follows.

To implement the real-time optimal control algorithm, the horizon T is divided into N steps, and the optimal control problem is discretized. The general discretized optimal control problem is formulated as

$$\begin{aligned}
&\min_{u} J = \sum_{i=0}^{N-1} L(x_i(\tau|t), u_i(\tau|t))\Delta\tau(t) \\
&\text{subject to} \\
&x_{i+1}(\tau|t) = x_i(\tau|t) + f(x_i(\tau|t), u_i(\tau|t))\Delta\tau(t) \\
&G(x_i(\tau|t), u_i(\tau|t)) \leq 0
\end{aligned} \tag{6.1.3}$$

where u is the control input, x is the state, L is the cost function. $f(x,u)$ is the state equation. $G(x,u)$ is the inequality constraint.

The inequality constraint in the optimal control problem is converted to an equality constraint by introducing a dummy input u_d for computation simplicity as follows:

$$C(x(t), u(t)) = u^2(t) + u_d^2(t) - u_{max}^2 = 0 \tag{6.1.4}$$

where u_{max} denotes the upper bound of the control input.

To solve this optimal control problem with the calculus of variation method [94], the Hamiltonian function is defined by

$$H(x, u, \lambda, \psi) = L(x, u) + \lambda^T f(x, u) + \psi^T C(x, u) \tag{6.1.5}$$

where λ denotes the co-state, and ψ denotes the Lagrange multiplier associated with the equality constraint.

The first-order necessary conditions for the optimal control input u, the multiplier ψ, and the co-state λ are obtained using the calculus of variation as

$$\begin{aligned}
&x_{i+1}(t) = x_i(t) + f(x_i(t), u_i(t))\Delta\tau(t) \quad x_0(t) = x(t) \\
&\lambda_i(t) = \lambda_{i+1}(t) + H_x(x_i(t), u_i(t), \lambda_{i+1}(t), \psi_i(t))\Delta\tau(t) \quad \lambda_N(t) = 0 \\
&H_u(x_i(t), u_i(t), \lambda_{i+1}(t), \psi_i(t)) = 0 \\
&C(x(t), u(t)) = 0
\end{aligned} \tag{6.1.6}$$

where x_0 is the initial state.

To solve this optimal control problem, the continuation and GMRES (C/GMRES) method is employed for computation cost reduction. The necessary conditions of optimality for the

constrained control input can be expressed as the following equation

$$
\begin{aligned}
&F(U(\tau|t), x(\tau|t), t) \\
&:= \begin{bmatrix} H_u(u_0(\tau|t), x_0(\tau|t), \lambda_1(\tau|t), \psi_0(\tau|t)) \\ C(u_0(\tau|t), x_0(\tau|t)) \\ \vdots \\ H_u(u_{N-1}(\tau|t), x_{N-1}(\tau|t), \lambda_N(\tau|t), \psi_{N-1}(\tau|t)) \\ C(u_{N-1}(\tau|t), x_{N-1}(\tau|t)) \end{bmatrix} = 0 \qquad (6.1.7) \\
&U(t) := [u_0^T(\tau|t), \psi_0^T(\tau|t), \cdots, u_{N-1}^T(\tau|t), \psi_{N-1}^T(\tau|t)]^T. \qquad (6.1.8)
\end{aligned}
$$

$F(U(t), x(t), t) = 0$ is identical to

$$
\begin{aligned}
&F(U(0), x(0), 0) := 0 \\
&\dot{F}(U, x, t) = -A_s F(U(t), x(t), t) \qquad (6.1.9)
\end{aligned}
$$

where A_s is a stable matrix introduced to stabilize $F = 0$. If F_U is nonsigular, a differential equation for $U(t)$ can be obtained as

$$
\dot{U} = -F_U^{-1}(A_s F - F_x \dot{x} - F_t) \qquad (6.1.10)
$$

The above differential equation can be solved by the GMRES method. The presented approach is also a kind of continuation method. The solution curve $U(t)$ is traced by integrating the above differential equation. Because there is no need to calculate the Jacobians and the linear equation iteratively, C/GMRES method assures the real time optimal control ability because of small computational cost. The detailed description of the solution for the

real-time optimal control algorithm can be found in [96].

BIBLIOGRAPHY

Bibliography

[1] M. Hori and T. Kaneda, "Effect of HEV and PHEV Share on Energy Demand/Supply Structure," *Transactions of Society of Automotive Engineers of Japan*, vol. 40, no. 4, pp. 1101–1106, 2009.

[2] S.W. Hadley and A.A. Tsvetkova, "Potential impacts of plug-in hybrid electric vehicles on regional power generation," *The Electricity Journal*, vol. 22, no. 10, pp. 56–68, Dec. 2009.

[3] N. Rajarajeswari and K. Thanushkodi, "Design of an intelligent bi-directional DC-DC converter with half bridge topology," *Journal of Applied Sciences Research*, vol. 4, no. 12, pp. 1618–1623, Sep. 2008.

[4] W. Kempton and J. Tomic, "Vehicle-to-grid power fundamentals: Calculating capacity and net revenue," *Journal of Power Source*, vol. 144, no. 1, pp. 268–279, 2005.

[5] B. K. Sovacool and R. F. Hirsh, "Beyond batteries: An examination of the benefits and barriers to plug-in hybrid electric vehicles (PHEVs) and a vehicle-to-grid (V2G) transition," *Energy Policy*, vol. 37, no. 3, pp. 1095–1103, March 2009.

[6] C. Pang, P. Dutta, and M. Kezunovic, "BEVs/PHEVs as Dispersed Energy Storage for V2B Uses in the Smart Grid," *IEEE Trans. Smart Grid*, vol. 3, no. 1, pp. 473–482, March 2012.

[7] A. Sciarretta and L. Guzzella, "Control of hybrid electric vehicles," *IEEE Control Syst. Mag.*, vol. 27, no. 2, pp. 60–70, Apr. 2007.

[8] S.J. Moura, H.K. Fathy, D.S. Callaway, and J.L. Stein, "A stochastic optimal control approach for power management in plug-in hybrid electric vehicles," *IEEE Trans. Control Syst. Technol.*, vol. 19, no. 3, pp. 545–555, May 2011.

[9] J. Liu and H. Peng, "Modeling and control of a power-split hybrid vehicle," *IEEE Trans. Control Syst. Technol.*, vol. 16, no. 6, pp. 1242–1251, Nov. 2008.

[10] P. Sharer, A. Rousseau, and D. Karbowski, "Plug-in Hybrid Electric Vehicle Control Strategy: Comparison between EV and Charge-Depleting Options," *SAE Technical Paper*, No. 2008-01-0460, 2008.

[11] C. Zhang and A. Vahidi, "Route preview in energy management of plug-in hybrid vehicles," *IEEE Trans. Control Syst. Technol.*, vol. 20, no. 2, pp. 546–553, March 2012.

[12] S. Delprat, T. M. Guerra, and J. Rimaux, "Control strategies for hybrid vehicles: Optimal control," *in Proc. Veh. Technol. Conf. (VTC 2002-Fall)*, pp.1681–1685, 2002.

[13] S. Delprat, T. M. Guerra, and J. Rimaux, "Optimal control of a parallel powertrain: From global optimization to real time control strategy," *in Proc. Veh. Technol. Conf.*, pp.2082–2088, 2002.

[14] S. Delprat, T. Guerra, G. Paganelli, J. Lauber, and M. Delhom, "Control strategy optimization for an hybrid parallel powertrain," *in Proc. Amer. Control Conf.*, pp.1315–1320, 2001.

[15] S. Bashash, S. J. Moura, J. C. Forman, and H. K. Fathy, "Plug-in Hybrid Vehicle Charge Pattern Optimization for Energy Cost and Battery Longevity," *Journal of Power Sources*, vol. 196, no. 1, pp. 541–549, Jan. 2012.

[16] I.V. Kolmanovsky, and D.P. Filev, "Terrain and traffic optimized vehicle speed control," *in Proc. IFAC Symp. Adv. Automotive Contr.*, 2010.

[17] N. Petit and A. Sciarretta, "Optimal drive of electric vehicles using an inversion-based trajectory generation approach," *in the 18th IFAC World Congress*, 2011.

[18] A. Sciarretta , L. Guzzella, and J. van Baalen, "Fuel optimal trajectories of a fuel cell vehicle," *in Proc. IFAC Int. Conf. Advances Vehicle Control Safety*, 2004.

[19] Y. He, S. M. Chowdhury, P. Pisu, and Y. Ma, "An energy optimization strategy for power-split drivetrain plug-in hybrid electric vehicles," *Transp. Res. Part C 22*, pp. 29–41, Jan. 2012.

[20] B. Zhang , C. C. Mi and M. Zhang, "Charge-depleting control strategies and fuel optimization of blended-mode plug-in hybrid electric vehicles," *IEEE Trans. Veh. Technol.*, vol. 60, no. 4, pp. 1516–1525, May. 2011.

[21] P. Tulpule , V. Marano, and G. Rizzoni, "Effects of different PHEV control strategies on vehicle performance," *in Proc. Amer. Control Conf.*, pp.3950–3955, 2009.

[22] V. H. Johnson, K. B. Wipke, and D. J. Rausen, "HEV control strategy for real-time optimization of fuel economy and emissions," *SAE Technical Paper*, No. 2000-01-1543, 2000.

[23] P. Tulpule , V. Marano, and G. Rizzoni, "Effects of different PHEV control strategies on vehicle performance," *in Proc. Amer. Control Conf.*, pp.3950–3955, 2009.

[24] S.-I. Jeon , S.-T. Jo , Y.-I. Park, and J.-M. Lee, "Multi-mode driving control of a parallel hybrid electric vehicle using driving pattern recognition," *Trans. ASME, J. Dyn. Syst. Meas. Control*, vol. 124, no. 1, pp. 141–149, March 2012.

[25] L. Serrao, *A comparative analysis of energy management strategies for hybrid electric vehicles.* PhD thesis, The Ohio State University, 2009.

[26] Q. Gong, P. Tulpule, V. Marano, S. Midlam-Mohler, and G. Rizzoni, "The role of ITS in PHEV performance improvement," *in Proc. Amer. Control Conf.*, pp.2119–2124, 2011.

[27] Y. Bin , Y. Li , Q. Gong, and Z.-R. Peng, "Multi-information integrated trip specific optimal power management for plug-in hybrid electric vehicles," *in Proc. Amer. Control Conf.*, pp.4607–4612, 2009.

[28] Q. Gong , Y. Li and Z.-R. Peng, "Optimal power management of plug-in HEV with intelligent transportation system," *in Proc. Int. Conf. Adv. Intell. Mechatron.*, pp.1–6, 2007.

[29] Q. Gong , Y. Li and Z.-R. Peng, "Computationally efficient optimal power management for plug-in hybrid electric vehicles based on spatial-domain two-scale dynamic programming," *in Proc. IEEE Int. Conf. Veh. Electron. Safety*, pp.90–95, 2008.

[30] Q. Gong , Y. Li and Z.-R. Peng, "Trip based power management of plug-in hybrid electric vehicle with two-scale dynamic programming," *in Proc. IEEE VPP Conf.*, pp.12–19, 2007.

[31] Q. Gong , Y. Li and Z.-R. Peng, "Trip based optimal power management of plug-in hybrid electric vehicles using gas-kinetic traffic flow model," *in Proc. Amer. Control Conf.*, pp.3225–3230, 2008.

[32] Q. Gong , Y. Li and Z.-R. Peng, "Power management of plug-in hybrid electric vehicles using neural network based trip modeling," *in Proc. Amer. Control Conf.*, pp.4601–4606, 2009.

[33] R. E. Bellman, *Dynamic Programming.* Princeton, NJ: Princeton Univ. Press, 1957.

[34] J. Liu and H. Peng, "Control optimization for a power-split hybrid vehicle," *in Proc. Amer. Control Conf.*, pp.466–471, 2006.

[35] N. Kim, S. Cha, and H. Peng. "Optimal control of hybrid electric vehicles based on Pontryagin's minimum principle," *IEEE Trans. Control Syst. Technol.*, vol. 19, no. 5, pp.1279–1287, Sept. 2011.

[36] S. Stockar , V. Marano , G. Rizzoni and L. Guzzella, "Optimal control for plug-in hybrid electric vehicles applications," *in Proc. Amer. Control Conf.*, pp.5024–5030, 2010.

[37] A. Chasse , G. Hafidi , P. Pognant-Gros and A. Sciarretta, "Supervisory control of hybrid powertrains: An experimental benchmark of offline optimization and online energy management," *in Proc. IFAC Workshop Engine Powertrain Control, Simulation Model.*, pp.110–117, 2009.

[38] L. Serrao and G. Rizzoni, "Optimal control of power split for a hybrid electric refuse vehicle," *in Proc. Amer. Control Conf.*, pp.4498–4503, 2008.

[39] L. Serrao , S. Onori, and G. Rizzoni, "ECMS as a realization of Pontryagin's minimum principle for HEV control," *in Proc. Amer. Control Conf.*, pp.3964–3969, 2009.

[40] C. Zhang, A. Vahidi, P. Pisu, X. Li, and K. Tennant, "Role of terrain preview in energy management of hybrid electric vehicles," *IEEE Trans. Veh. Technol.*, vol. 59, no. 3, pp. 1139–1147, Mar. 2010.

[41] G. Paganelli, Y. Guezennec, and G. Rizzoni, "Optimizing control strategy for hybrid fuel cell vehicle," *SAE Technical Paper*, No. 2002-01-0102, 2002.

[42] C. Musardo , G. Rizzoni and B. Staccia, "A-ECMS: an adaptive algorithm for hybrid electric vehicle energy management," *in Proc. 44th IEEE Conf. Decision Control, 2005 European Control Conf.*, pp. 1816–1823, 2005.

[43] A. Chasse, G. Hafidi, P. Pognant-Gros, and A. Sciarretta, "Supervisory control of hybrid powertrains: An experimental benchmark of offline optimization and online energy management," *in Proc. IFAC Workshop Engine Powertrain Control, Simulation Model.*, pp. 110–117, 2009.

[44] J. Liu, H. Peng, and Z. Filipi, "Modeling and analysis of the Toyota hybrid system," *in Proc. Int. Conf. Advanced Intell. Mechatron.*, pp.134-139, 2005.

[45] M. Koot, J. T. B.A. Kessels, B. de Jager, W. P. M. H. Heemels, P. P. J. van den Bosch, and M. Steinbuch, "Energy management strategies for vehicular electric power systems,", *IEEE Trans. Veh. Technol.*, vol. 54, no. 3, pp. 771–782, May 2005.

[46] S. Kermani, S. Delprat, T.M. Guerra, R. Trigui, and B. Jeanneret, "Predictive energy management for hybrid vehicle," *Control Eng. Pract.*, vol. 20, no. 4, pp. 408–420, Apr. 2012.

[47] S. Schepmann and A. Vahidi, "Heavy vehicle fuel economy improvement using ultracapacitor power assist and preview-based MPC energy management," *in Proc. Amer. Control Conf.*, pp.2707–2712, 2011.

[48] S. Kermani, S. Delprat, R. Trigui, and T. M. Guerra, "Predictive energy management of hybrid vehicle," *Proc. IEEE Veh. Power Propuls. Conf.*, pp. 1–6, 2008.

[49] G. Ripaccioli, D. Bernardini, S. Di Cairano, A. Bemporad, and I. Kolmanovsky, "A stochastic model predictive control approach for series hybrid electric vehicle power management," *in Proc. Amer. Control Conf.*, pp.5844–5849, 2010.

[50] T.S. Kim, C. Manzie, and R. Sharma, "Model predictive control of velocity and torque split in a parallel hybrid vehicle," *in the IEEE International Conference on Systems, Man and Cybernetics*, pp.2014–2019, 2009.

[51] M. Back, M. Simons, F. Kirschbaum, and V. Krebs, "Predictive control of drivetrains," *in Proc. 15th IFAC World Congress*, 2002.

[52] L. Johannesson, S. Pettersson, and B. Egardt, "Predictive energy management of a 4QT series-parallel hybrid electric bus," *Control Eng. Pract.*, vol. 17, no. 12, pp. 1440–1453, Dec. 2009.

[53] M. Debert, G. Colin, Y. Chamaillard, L. Guzzella, A. Ketfi-Cherif, and B. Bellicaud, "Predictive energy management for hybrid electric vehicles-Prediction horizon and battery capacity sensitivity," *in Proc. IFAC Int. Conf. Advances Vehicle Control Safety*, 2010.

[54] H. Borhan, A. Vahidi, A.M. Phillips, M.L. Kuang, I.V. Kolmanovsky, and S.D. Cairano, "MPC-based energy management of a power-split hybrid electric vehicle," *IEEE Trans. Control Syst. Technol.*, vol. 20, no. 3, pp. 593–603, May 2012.

[55] H. Borhan and A. Vahidi, "Model predictive control of a power-split hybrid electric vehicle with combined battery and ultracapacitor energy storage," *in Proc. Amer. Control Conf.*, pp.5031–5036, 2010.

[56] H. Borhan, C. Zhang, A. Vahidi, A. Phillips, M. Kuang, and S. Di Cairano, "Nonlinear model predictive control for power-split hybrid electric vehicles," *in Proc. 49th IEEE Conf. on Decision and Control*, pp.4890–4895, 2010.

[57] H. Borhan , A. Vahidi , A. Phillips , M. Kuang and I. Kolmanovsky, "Predictive energy management of a power-split hybrid electric vehicle," *in Proc. Amer. Control Conf.*, pp.3970–3976, 2009.

[58] Y. Deguchi and T. Kawabe, "HEV charge/discharge control system based on navigation information," *SAE Technical Paper*, No. 2004-21-0028, 2004.

[59] S. Stockar, V. Marano, M. Canova, G. Rizzoni, and L. Guzzella, "Energy-optimal control of plug-in hybrid electric vehicles for real-world driving cycles," *IEEE Trans. Veh. Technol.*, vol. 60, no. 7, pp. 2949 -2962, Sept. 2011.

[60] Q. Gong and Y. Li, "Trip based optimal power management of plug-in hybrid electric vehicle with advanced traffic modeling," *SAE Technical Paper*, No. 2008-01-1316, 2008.

[61] Q. Gong, Y. Li, and Z. Peng, "Trip-based optimal power management of plug-in hybrid electric vehicles," *IEEE Trans. Veh. Technol.*, vol. 57, no. 6, pp. 3393–3401, Nov. 2008.

[62] L. Guzzella and A. Sciarretta, *Vehicle Propusion Systems: Introduction to Modeling and Optimization.* New York: Springer, 2005.

[63] A. Sciarretta, M. Back, and L. Guzzella, "Optimal control of parallel hybrid electric vehicles,", *IEEE Trans. Control Syst. Technol.*, vol. 12, no. 3, pp. 352–363, May 2004.

[64] C. Zhang and A. Vahidi, "Real-time optimal control of plug-in hybrid vehicles with trip preview," *in Proc. Amer. Control Conf.*, pp. 6917–6922, 2010.

[65] C. Zhang, A. Vahidi, X. Li, and D. Essenmacher, "Role of trip information preview in fuel economy of plug-in hybrid vehicles," *in Proc. ASME*, pp. 253–258, 2009.

[66] C. Zhang, A. Vahidi, P. Pisu, X. Li, and K. Tennant, "Utilizing road grade preview for increasing fuel economy of hybrid vehicles," *in Proceedings of the 12th IFAC Symposium on Transportation Systems*, pp. 168–173, 2009.

[67] A. Sciarretta, L. Guzzella, and M. Back, "A real-time optimal control strategy for parallel hybrid vehicles with on-board estimation of the control parameters," *in Proc. IFAC Symp. Adv. Automotive Contr.*, 2004.

[68] A. Sciarretta, L. Guzzella, C. H. Onder, "On the power split control of parallel hybrid vehicles: from global optimization towards real-time control," *Automatisierungstechnik*, vol. 51, no. 5, pp. 195–203, May 2003.

[69] D. Ambuhl and L. Guzzella, "Predictive reference signal generator for hybrid electric vehicles," *IEEE Trans. Veh. Technol.*, vol. 58, no. 9, pp. 4730–4740, Nov. 2009.

[70] N. Petit and A. Sciarretta, "Optimal drive of electric vehicles using an inversion-based trajectory generation approach," *in the 18th IFAC World Congress*, 2011.

[71] G. Paganelli, S. Delpart, T.M. Guerra, J. Rimaux, and J.J. Santin, "Equivalent consumption minimization strategy for parallel hybrid powertrains," *Proc. Veh. Technol. Conf.*, pp. 2076–2081, 2002.

[72] D. Yamaguchi, M. Kamal, M. Mukai, and T. Kawabe, "Model predictive control for automobile ecological driving using traffic signal information," *Journal of System Design and Dynamics*, vol. 6, no. 3, pp. 297–309, Jun. 2012.

[73] M. Kamal, M. Mukai, J. Murata, and T. Kawabe, "Ecological vehicle control on roads with up-down slopes," *IEEE Trans. Intell. Transp. Syst.*, vol. 12, no. 3, pp. 783–794, Sept. 2011.

[74] K. Yu, M. Mukai, and T. Kawabe, "Performance of an eco-driving nonlinear MPC system for a power-split HEV during car following," *The 13th SICE Control Division Conference*, Fukuoka, Japan, March 2013.

[75] K. Yu, M. Mukai, and T. Kawabe, "Model predictive control of a power-split hybrid electric vehicle system," *The 17th International Symposium on Artificial Life and Robotics*, Beppu, Japan, Jan. 2012.

[76] M. Kamal, M. Mukai, J. Murata, and T. Kawabe, "Ecological driver assistance system using model-based anticipation of vehicle-road-traffic information," *IET Intelligent Transportation systems*, vol. 4, no. 4, pp. 244–251, Dec. 2010.

[77] M. Kamal, M. Mukai, J. Murata, and T. Kawabe, "Ecological Driving Based on Preceding Vehicle Prediction Using MPC," *in the 18th IFAC World Congress*, pp. 3843–3848, 2011.

[78] M. Kamal, M. Mukai, J. Murata, and T. Kawabe, "On board eco-driving system for varying road-traffic environments using model predictive control," *in the IEEE International Conference on Control Applications*, pp. 1636–1641, 2010.

[79] M. Kamal, M. Mukai, J. Murata, and T. Kawabe, "Development of ecological driving assist system - model predictive approach in model predictive approach in vehicle control," *in the Proc. Of the 16th ITS-World Congress*, 2009.

[80] M. Kamal, M. Mukai, J. Murata, and T. Kawabe, "Model predictive control of vehicles on urban roads for improved fuel economy ," *IEEE Trans. Contr. Syst. Technol.*, vol. 21, no. 3, pp. 831–841, May. 2013.

[81] K. Yu, M. Mukai, and T. Kawabe, "Model predictive control of a power-split hybrid electric vehicle system," *Artificial Life and Robotics*, vol. 17, no. 2, pp. 221–226, Dec. 2012.

[82] K. Yu, M. Mukai, and T. Kawabe, "A battery management system using nonlinear model predictive control for a hybrid electric vehicle," Accepted in *the 7th IFAC Symposium on Advances in Automotive Control.*

[83] E. Hellstrom, M. Ivarsson, J. Aslund and L. Nielsen, "Look-ahead control for heavy trucks to minimize trip time and fuel consumption," *Control Eng. Pract.*, vol. 17, no. 2, pp. 245–254, Feb. 2009.

[84] A. Vahidi and A. Eskandarian, "Research advances in intelligent collision avoidance and adaptive cruise control," *IEEE Trans. Intell. Transp. Syst.*, vol. 4, no. 3, pp. 783–794, Sep. 2003.

[85] D. Swaroop, J.K. Hedrick, C.C. Chien, and P. Iannou, "A comparison of spacing and headway control laws for automatically controlled vehicles," *Vehicle Syst. Dynamics J.*, vol. 23,no. 8, pp. 597–625. Nov. 1994.

[86] J. Kim, N. Kim, S. Hwang, Y. Hori, and H. Kim, "Motor control of input-split hybrid electric vehicle," *Int. J. Automotive Technol*, vol. 10, no. 6, pp. 733–742, Dec. 2009.

[87] J. Barkenbus, "Eco-driving: An overlooked climate change initiative," *Energy Policy*, vol. 38, no. 2, pp. 762–769, 2010.

[88] Y. Yasui, "JSAE-SICE benchmark problem2: fuel consumption optimization of commuter vehicle using hybrid powertrain," in *Proceedings of 10th World Congress Intelligent Control Automation*, 2012, pp. 606-611.

[89] Y. Yasui, "Benchmark problem 2: fuel consumption optimization of commuter vehicle using hybrid powertrain," *JSAE Annual Congress (Spring)*, 2011 (in Japanese).

[90] C.C. Lin, H. Peng, J.W. Grizzle, and J.M. Kang, "Power management strategy for a parallel hybrid electric truck," *IEEE Trans. Contr. Syst. Technol.*, vol. 11, no. 6, pp. 839–849, Nov. 2003.

[91] K.B. Wipke, M.R. Cuddy, and S.D. Burch, "ADVISOR 2.1: a user-friendly advanced powertrain simulation using a combined backward/forward approach," *IEEE Trans. Veh. Technol.*, vol. 48, no. 6, pp. 1751–1761, Nov. 1999.

[92] M. Ehsani, Y. Gao, and A. Emadi, *Modern Electric, Hybrid Electric, and Fuel Cell Vehicles: Fundamentals, Theory, and Design*, 2rd ed. Boca Raton, FL: CRC, 2009.

[93] G. Rizzoni, L. Guzzella, and B. Baumann, "Unified modeling of hybrid electric vehicle drivetrains," *IEEE/ASME Trans. Mechatron.*, vol. 4, no. 3, pp.246–257, Sept. 1999.

[94] D.E. Kirk, *Optimal Control Theory: an Introduction.* Englewood Cliffs, NJ: Prentice-Hall, 1970.

[95] J.M. Maciejowski, *Predictive Control with Constraints.* Englewood Cliffs, NJ: Prentice-Hall, 2002.

[96] T. Ohtsuka, "A continuation/GMRES method for fast computation of nonlinear receding horizon control," *Automatica*, vol. 40, no. 4, pp. 563–574, Apr. 2004.

[97] K. Muta, M. Yamazaki, and J. Tokieda. "Development of new-generation hybrid system THS II–Drastic improvement of power performance and fuel economy," *SAE Technical Paper*, No. 2004-01-0064, 2004.

[98] K. Ahn, S. Cho, and S.W. Cha, "Optimal operation of the power-split hybrid electric vehicle powertrain," *Proc. IMechE, Pt. D: J. Automobile Eng.*, vol. 222, no. 5, pp. 789–800, 2008.

[99] M. Schulz, "Set values for a power-split hybrid electric vehicle through numerical optimization," *Int. J. Alternative Propulsion*, vol. 1, no. 1, pp. 6–31, 2006.

[100] K. Ahn and P. Y. Papalambros, "Engine optimal operation lines for power-split hybrid electric vehicles," *Proc. IMechE, Pt. D: J. Automobile Eng.*, vol. 223, no. 9, pp. 1149–1162, 2009.

[101] H.N. Gupta, *Fundamentals of internal combustion engines.* NewDelhi: Prentice-Hall of India, 2006.

[102] D. Rotenberg, A. Vahidi, and I. Kolmanovsky, "Ultracapacitor assisted powertrains: modeling, control, sizing, and the impact on fuel economy," *IEEE Trans. Control Syst. Technol.*, vol. 19, no. 3, pp. 576–589, May 2011.